

# Spectroscopy of Neurotransmitters and Their Clusters: Phenethylamine and Amphetamine Solvation by Nonpolar, Polar, and Hydrogen-Bonding Solvents

J. Yao, H. S. Im, M. Foltin, and E. R. Bernstein\*

Department of Chemistry, Colorado State University, Fort Collins, Colorado 80523-1872

Received: February 1, 2000; In Final Form: April 17, 2000

Clusters containing a phenylethylamine (PEA) or amphetamine (AMP) molecule and a solvent species such as Ar, CH<sub>4</sub>, CF<sub>3</sub>H, CO<sub>2</sub>, H<sub>2</sub>O, and other small molecules are formed in a supersonic jet expansion. Spectral studies of the solvation and related chemistry of PEA and AMP are pursued by using both fluorescence and mass spectroscopy techniques. To help analyze the experimental results, ab initio and atom–atom Lennard-Jones–Coulomb (LJC) potential calculations are employed to calculate cluster geometries and binding energies. The LJC potential parameters for the 10–12 hydrogen-bonding potentials have been reevaluated on the basis of new ab initio partial atomic charge values and new experimental binding energies and geometries. The observed dependence of the relative spectral intensities of PEA and AMP conformers and their clusters on the cooling conditions (backing pressure and coolants employed) suggests that these species undergo population redistribution in the cooling and clustering process. The amount of excess energy (binding energy) available to the forming cluster plays a major role in the conformational conversion of PEA and AMP during cluster formation. If strong interactions (hydrogen bonding) exist between the solute and the solvent, such conversion/redistribution processes occur among all conformers and their clusters. The conversion/redistribution process is restricted within the anti or gauche conformer sets and their clusters for weakly interacting solute/solvent pairs. All PEA and AMP clusters studied experience complete fragmentation upon ionization. The observed gradual dependence of photo ion intensity on the ionization laser energy suggests a significant change in geometry for both PEA and AMP, as well as their clusters, upon ionization. Consequently the high vertical ionization energy leads to an excess energy in the vibrational modes of the ions, causing fragmentation of the clusters. The clusters can fragment along two different general paths: (1) simple loss of the solvent molecules and (2) breaking the  $\alpha$ – $\beta$  carbon bond of PEA or AMP, with additional loss of solvent molecules in some cases. Those clusters with weaker solute/solvent binding tend to fragment through solvent loss, while those forming hydrogen bonds tend to favor the  $\alpha$ – $\beta$  carbon bond cleavage. Reactions are observed for PEA and AMP with NO. NO can completely quench PEA and AMP monomer spectra. The reaction products include C<sub>6</sub>H<sub>5</sub>CH=CH<sub>2</sub> and C<sub>6</sub>H<sub>5</sub>NH<sub>2</sub> for PEA and C<sub>6</sub>H<sub>5</sub>CH=CHCH<sub>3</sub> and C<sub>6</sub>H<sub>5</sub>NH<sub>2</sub> for AMP.

## I. Introduction

Phenethylamine (C<sub>6</sub>H<sub>5</sub>C<sub>2</sub>H<sub>4</sub>NH<sub>2</sub>, PEA) serves as the fundamental structural unit for a number of very important neurotransmitters. These include amphetamine (C<sub>6</sub>H<sub>5</sub>CH<sub>2</sub>CH(CH<sub>3</sub>)-NH<sub>2</sub>, AMP), dopamine, noradrenaline, adrenaline, and others. PEA and AMP are the simplest members of this class of neurotransmitters with regard to structure, solvation, and chemistry, and are thereby good molecules to access initially for a detailed study of the conformational and solvation properties of neurotransmitters.

In the past decade or so, a number of studies of the conformation and electronic spectroscopy of PEA have appeared.<sup>1–6</sup> Most of the past interest has been focused on the conformation of PEA isolated in a supersonic jet expansion and cooled to a low internal and rotational temperature. For example, Sulkes and co-workers<sup>1</sup> and Levy and co-workers<sup>2</sup> identified four major S<sub>1</sub> ← S<sub>0</sub> transition origins for PEA conformers in the 37 600 cm<sup>-1</sup> region. These transitions are assigned by Levy and co-workers to two anti and two gauche conformers of PEA. The conformational structure of PEA has been further studied by Godfrey et al.<sup>3</sup> using microwave spectroscopy and ab initio

calculation at the HF/6-31G\*\* and MP2/6-31G\*\* levels. The two gauche conformers B and C and the two anti conformers A and D assigned by Levy et al.<sup>2</sup> correspond to the II, III, IV, and V conformer structures identified by Godfrey et al.<sup>3</sup> Recent work by Dickinson et al.,<sup>5</sup> using laser-induced fluorescence and mass-resolved excitation spectroscopies and ab initio calculations, is also consistent with these results.

In addition to the conformations of isolated PEA, another important aspect of recent studies deals with the solvation behavior of the various conformers of PEA. For example, a solvent such as water may readily bind to each of the PEA conformers, and such binding may occur at either the top or bottom of the phenyl ring or near the amine group away from the ring  $\pi$  system. Cluster studies, especially by electronic (S<sub>1</sub> ← S<sub>0</sub>) spectroscopy, often involve mass-resolved detection of the cluster species, and fragmentation of the cluster can occur directly following the vertical ionization process employed for mass spectroscopy. Cluster fragmentation can occur (as we shall discuss) into a number of different mass channels, and this loss of clear mass identity for a given feature in the electronic spectrum of PEA/solvent clusters complicates the experimental study of PEA solvation. In our previous work<sup>4</sup> on PEA conformers, one of the spectral features that appears in both

\* To whom correspondence should be addressed.

fluorescence excitation spectra and mass-resolved excitation spectra of PEA was assigned as the fifth conformer of PEA; however, as was later pointed out by Dickinson et al.,<sup>5</sup> and as we shall see in this paper, this “fifth PEA feature” arises from a PEA(H<sub>2</sub>O)<sub>1</sub> cluster. A careful cluster formation and fragmentation study demands very detailed analysis of mass-resolved excitation spectra collected in the cluster parent mass channel (if possible) and in all possible fragment mass channels. As a continuation of the work of Dickinson et al.,<sup>5</sup> a recent report by Hockridge et al.<sup>6</sup> details the fragmentation of PEA(H<sub>2</sub>O)<sub>1</sub> clusters. Both theory and experiment are presented in this latter reference, and some cluster structural information can be suggested.

A similar set of investigations has apparently not been undertaken for other neurotransmitter species in this series, such as AMP. In this work, we investigate the solvation behavior of both PEA and AMP with polar, nonpolar, and hydrogen-bonding solvents. Fluorescence excitation spectroscopy is employed for general survey of the spectra of bare PEA and AMP, as well as for all the clusters. We then proceed to employ both one- and two-color mass-resolved excitation spectroscopy (MRES) to investigate the spectra of all species in their parent and all possible fragment mass channels. Due to extensive fragmentation and dissociation upon ionization, in almost all instances, clusters are not directly detected in their parent mass channels. The assignment of cluster electronic spectra to specific cluster sizes is thus based on less than optimal information. We consider the following five criteria. First, and perhaps most obvious, is that the first cluster features to appear at very low solvent molecule concentration in the expansion gas (<0.1% in general and for water ca. 10 ppm) belong to one-to-one solute/solvent clusters. Features for larger clusters appear as the solvent concentration is increased. Second, the time delay between pulsed nozzle opening and the appearance of a signal for a given mass species depends on the mass of the parent neutral species generated at the nozzle by cluster growth. Thus, the first species to arrive at the ionization region for maximum signal intensity is the monomer. This is closely followed by the one-to-one-cluster, etc., in a regular series of time steps due to cluster formation time differences and velocity slip in the beam.<sup>7</sup> We have used this “arrival time delay” to determine cluster sizes of a number of fragmenting species (toluene/water, DABCO/Ar<sub>n</sub>, benzyl alcohol/H<sub>2</sub>O, benzyl alcohol/NH<sub>3</sub>, and others). Third, clusters will fragment along different paths and will have spectra that correlate between different mass channels. We look for this mass correlation to determine the parent cluster and how it behaves with regard to fragmentation. Fourth, changes in ionization energy will change the relative rates of fragmentation of a parent cluster into different daughter species, and these species can be observed to correlate in intensity for different daughters. Again, the daughter–daughter correlation can often be used to uncover a parent cluster. Fifth, careful identification of monomer vibronic features and impurities is needed since all the clusters fragment completely upon ionization. Given these criteria, one is hopeful that a consistent picture of cluster behavior, structure, and fragmentation patterns for all detected species can be generated. On the basis of a detailed analysis of both the mass and optical spectra of this set of clusters, and theoretical modeling of cluster structure, one can generate paths for cluster formation, fragmentation, and chemistry.

Theoretical modeling of van der Waals clusters becomes an essential component of the data analysis process as the experimental data for these larger systems are not complete; that is, completely resolved rotational features are presently not

available for PEA/solvent or AMP/solvent clusters. Both solvation behavior and chemical reaction can be modeled in this manner. Two approaches have been taken over the years to elucidate the structure and chemistry of van der Waals clusters: empirical and semiempirical potential energy surface simulation, and ab initio quantum chemical calculations.

For the past two decades, solvation properties of clusters (binding energy, geometry, vibrations, etc.) have been well estimated by semiempirical potential energy calculations. Cluster systems studied include both open and closed shell systems containing aromatic and nonaromatic solute chromophores.<sup>8–10</sup>

More recently, ab initio approaches to the elucidation of intermolecular interactions have been explored. To obtain acceptable results (e.g., binding energies to  $\pm 100$  cm<sup>-1</sup> or <4 kJ/mol), a very high level of calculation and basis set sophistication is demanded.<sup>11</sup> With the rapidly increasing growth of computational power, structures of clusters such as (CH<sub>4</sub>)<sub>2</sub>, (H<sub>2</sub>O)<sub>2</sub>, (NH<sub>3</sub>)<sub>2</sub>, NH<sub>3</sub>(H<sub>2</sub>O), and CH<sub>4</sub>(NH<sub>3</sub>) can be obtained and geometry optimized at the MP2/cc-pVTZ and CCSD(T)/cc-pVTZ levels. Such an approach does give useful results that agree well with extant experimental data. Nevertheless, such high-level calculations are still too expensive to pursue for cluster systems of large molecules, such as PEA and AMP. Hockridge et al.<sup>6</sup> present MP2/6-31G\* level calculations with HF level basis set superposition error (BSSE) corrections for the PEA(H<sub>2</sub>O)<sub>1</sub> clusters. Given that the basis set is so small, and that the BSSE at this level is at least ca. 3 kcal/mol, one cannot have very high confidence in the accuracy of the solvation properties for PEA thus calculated, although they appear to be qualitatively correct. For systems such as PEA(Ar)<sub>1</sub> and PEA(CH<sub>4</sub>)<sub>1</sub>, the cluster binding is much weaker and thus more difficult to calculate from the ab initio approach.<sup>11</sup> A good ab initio estimation of such weak interactions is still beyond current capabilities for systems with so many heavy atoms. Thereby, in this work we employ semiempirical potential energy surface calculations to model the van der Waals clusters accessed by the electronic spectroscopy techniques described above.

## II. Procedures

**A. Experimental Details.** Both fluorescence excitation (FE) spectroscopy and MRES are described in detail in previous publications from this laboratory.<sup>10,12</sup> Only a brief description of some of the particular details associated with the systems of interest is presented herein.

For FE, a General Valve pulsed nozzle is employed to generate the supersonic expansion into a stainless steel vacuum chamber, while for MRES, an R. M. Jordan pulsed nozzle is employed. Liquid PEA (Aldrich) or AMP (Sigma) is placed in a glass ampule located close to the nozzle throat, and is slightly warmed to increase the vapor pressure of the sample. The expansion gas is He at ca. 100–200 psig. Solvent gas is mixed into the expansion gas, and clusters form as the mixture cools in the adiabatic expansion from the nozzle into the vacuum chamber.

In FE experiments, a Nd:YAG pumped dye laser is used as the laser excitation source for the neurotransmitter monomers and their clusters. The laser output of LDS 698 (Exciton) dye in methanol is doubled and mixed with the Nd:YAG laser fundamental output (1064 nm) to achieve the appropriate wavelength range. This laser beam intersects the molecular beam about 15 mm downstream from the nozzle exit. Fluorescence is collected with a 5 cm focal length lens and is focused on a C31034A RCA photomultiplier tube cathode in a direction perpendicular to the coplanar laser and molecular beams.

Both one- and two-color experiments are performed for MRES detection of the bare molecules and their clusters. For the one-color MRES, the laser used is the same as above. The total excitation and ionization energy is ca.  $75\,000\text{ cm}^{-1}$  in this instance. For a two-color experiment, a second Nd:YAG pumped dye laser is used as the ionization source ( $I \leftarrow S_1$ ). The total two-color energy is ca.  $72\,000\text{ cm}^{-1}$ , just enough to ionize PEA, AMP, and their weakly bound clusters (e.g.,  $\text{PEA}(\text{Ar})_1$ ,  $\text{PEA}(\text{CH}_4)_1$ , etc.). The doubled output of a Kiton Red and Rhodamine 640 (both from Exciton) mixture in methanol is used to cover the appropriate wavelength range for the ionization laser. MRES detection of ionized species is achieved by a Galileo Electro-optics microchannel plate detector at the end of a 1.5 m flight tube.

**B. Theoretical Details.** The solvation properties of PEA and AMP clusters are analyzed in this study using a semiempirical Lennard-Jones–Coulomb (LJC) potential model. The potential energy function is given by<sup>13</sup>

$$E = \sum_{i=1}^n \sum_{j=1}^m \left\{ \left( \frac{A_{ij}}{r_{ij}^{12}} - \frac{C_{ij}}{r_{ij}^6} \right) (1 - \delta_{ij}^{\text{hb}}) + \frac{q_i q_j}{D r_{ij}} + \left( \frac{A_{ij}^{\text{hb}}}{r_{ij}^{12}} - \frac{C_{ij}^{\text{hb}}}{r_{ij}^{10}} \right) \delta_{ij}^{\text{hb}} \right\} \quad (1)$$

in which

$$A_{ij} = C_{ij} r_{\text{min}}^6 / 2 \quad \text{and} \quad C_{ij} = \frac{3/2 e (\hbar/m^{1/2}) \alpha_i \alpha_j}{(\alpha_i/N_i)^{1/2} + (\alpha_j/N_j)^{1/2}} \quad (2)$$

In these equations  $e$  and  $m$  are the electron charge and mass, and  $q_i$  and  $q_j$  are partial atomic charges for the atoms of the solute and solvent, respectively.  $D$  is the dielectric constant parameter,<sup>13</sup>  $r_{ij}$  is the distance between atoms  $i$  and  $j$  of two different molecules in the cluster,  $\alpha_i$  is the atomic polarizability of atom  $i$ ,  $N_i$  is the effective number of electrons for each atom type,  $r_{\text{min}} = (r_{ii} + r_{jj})/2$ , and  $r_{ii}$  and  $r_{jj}$  are twice the van der Waals radii of the atoms in the cluster. The  $\alpha_i$  and  $N_i$  are obtained from ref 13, and the  $q_i$  are calculated as discussed below. The summation in eq 1 is taken so as not to double count any of the atom–atom pairwise interactions for the cluster.  $\delta_{ij}^{\text{hb}}$  is an accounting device that allows hydrogen-bonding interactions ( $\delta_{ij}^{\text{hb}} = 1$ ) to be modeled as appropriate by the potential energy function. For non-hydrogen-bonding situations  $\delta_{ij}^{\text{hb}} = 0$ .

Given the potential function, the task is to find appropriate parameters for the various terms. For ground-state clusters, atomic polarizabilities and atomic van der Waals radii can be found in the literature.<sup>13–15</sup> The partial atomic charges and geometry of the PEA, AMP, and solvents need to be calculated.

To simplify the modeling, and to employ transferable potential parameters and molecular geometries, the relaxation of geometry and atomic charge distribution of each molecule in a cluster system are neglected: the geometry and atomic charges of isolated molecules are employed in the modeling.

Atomic charges for solute and solvent species are calculated separately employing the ab initio quantum chemistry package Gaussian 98.<sup>16</sup> Since the structure of all the solvents is known and they remain in their ground electronic and vibrational state during the experiment, a single-point calculation at the MP2 level with an aug-cc-pVDZ or larger basis set is employed to obtain their atomic charges.<sup>10</sup> Geometry optimization and atomic charge calculations are performed at the MP2/6-311++G\*\* level for PEA conformers, and at the MP2/6-31++G\*\* level for AMP conformers. The atomic charges on the solute and solvent atoms are calculated using the electrostatic potential grid

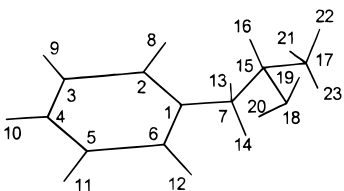
**TABLE 1: Atomic Charges of Various Solvent Molecules by ab Initio Calculation Using Gaussian 98 at MP2 Level**

molecule	basis set	dipole moment (D)		atom	charge
		calcd	exptl <sup>a</sup>		
H <sub>2</sub> O	aug-cc- pVTZ	1.913	1.854	O	−0.678
				H	0.339
	aug-cc- pVQZ	1.917	1.854	O	−0.680
				H	0.340
(H <sub>2</sub> O) <sub>2</sub> <sup>b</sup>	aug-cc- pVTZ			O <sub>donor</sub>	−0.754
				H <sub>donor</sub>	0.361
				H <sub>H–bond</sub>	0.358
				O <sub>acceptor</sub>	−0.705
				H <sub>acceptor</sub>	0.370
				H <sub>acceptor</sub>	0.370
NH <sub>3</sub>	aug-cc- pVTZ	1.587	1.471	N	−0.867
				H	0.289
	aug-cc- pVDZ	1.607	1.471	N	−0.857
				H	0.286
CH <sub>4</sub>	aug-cc- pVDZ	0.0	0.0	C	−0.303
				H	0.076
CF <sub>4</sub>	aug-cc- pVDZ	0.0	0.0	C	0.680
				F	−0.170
CF <sub>3</sub> H	aug-cc- pVDZ	1.726	1.651	C	0.555
				F	−0.205
				H	0.060
CO <sub>2</sub>	aug-cc- pVDZ	0.0	0.0	C	0.748
				O	−0.374
CH <sub>3</sub> OH	aug-cc- pVDZ	1.667	1.70	C	0.289
				H <sub>CH<sub>3</sub></sub>	−0.01
				O	−0.628
				H <sub>OH</sub>	0.384

<sup>a</sup> Reference 14. <sup>b</sup> The donor and acceptor indicate proton donor and acceptor, respectively.

fitting method (ChelpG Scheme). This method has been shown to give useful convergent atomic charges for intermolecular potential energy calculations.<sup>10,17</sup> Calculated  $q_i$  values of some typical solvent molecules employed in these studies are presented in Table 1. The atomic charges calculated for the C conformers of PEA and AMP are listed in Table 2.

As emphasized in previous reports from our laboratory<sup>10</sup> and others<sup>8,9</sup> and, indeed in this work as well, modeling of ground-state properties of van der Waals weakly bound clusters is generally quite successful; however, our initial attempts to fit hydrogen-bonding interactions using the hydrogen-bonding potential parameters of ref 13 were much less successful. For example, experimental<sup>18</sup> and ab initio<sup>16,19</sup> results suggest that the water dimer ((H<sub>2</sub>O)<sub>2</sub>) has a binding energy of ca. 20.5 kJ/mol, and a ca. 175° angle for the O–H···O hydrogen bond direction with newly calculated (and accepted) atomic charges and geometry,<sup>11,19</sup> but using the hydrogen-bonding (10–12 potential) parameters  $A_{ij}^{\text{hb}}$  and  $C_{ij}^{\text{hb}}$ ,<sup>13</sup> the calculated binding energy is 50% higher than the above result, and the dimer geometry is of high symmetry with two hydrogen atoms of one H<sub>2</sub>O molecule (the electron acceptor or hydrogen donor) equally bound to the oxygen atom of the other H<sub>2</sub>O molecule (the electron donor or hydrogen acceptor). See Table 1. The cause of such a failure of the potential model for the “hydrogen-bonding” interaction is mainly due to the inadequacy of the tabulated  $A^{\text{hb}}$  and  $C^{\text{hb}}$  parameters for the 10–12 potential. These parameters were derived using Mulliken charges at the CINDO level to estimate the Coulomb interactions. The Mulliken charges at the CINDO level are much smaller than the ones presently viewed as appropriate on the basis of fitting charges to an electrostatic potential at the high theoretical level mentioned above for H<sub>2</sub>O and other molecules (see Table 1). The original Coulomb interactions were thus greatly underestimated, and the  $A_{ij}^{\text{hb}}$  and  $C_{ij}^{\text{hb}}$  parameters thus derived are not appropriate to be

**TABLE 2: Atomic Charges of C Conformers of PEA and AMP by ab Initio Calculation Using Gaussian 94 at the MP2 Level<sup>a</sup>**


PEA				AMP	
number	atom	6-311++G**	aug-cc-pVDZ	atom	6-311++G**
1	C	0.169 212	0.183 945	C	0.166 616
2	C	-0.142 181	-0.165 576	C	-0.172 113
3	C	-0.116 420	-0.095 120	C	-0.086 133
4	C	-0.085 105	-0.095 044	C	-0.091 361
5	C	-0.1134 43	-0.094 196	C	-0.096 910
6	C	-0.113 643	-0.130 340	C	-0.112 118
7	C	-0.279 072	-0.266 487	C	-0.287 987
8	H	0.111 186	0.114 865	H	0.110 968
9	H	0.090 740	0.085 891	H	0.083 190
10	H	0.089 741	0.087 542	H	0.085 911
11	H	0.093 004	0.087 058	H	0.084 543
12	H	0.092 599	0.096 197	H	0.094 360
13	H	0.030 763	0.030 884	H	0.039 106
14	H	0.081 248	0.075 604	H	0.065 808
15	C	0.585 966	0.557 588	C	0.768 500
16	H	-0.133 539	-0.128 690	H	-0.169 361
17	H	-0.039 844	-0.040 625	C	-0.217 427
18	N	-0.972 324	-0.902 298	N	-1.049 110
19	H	0.335 628	0.313 113	H	0.352 475
20	H	0.315 484	0.285 692	H	0.322 039
21				H	0.023 081
22				H	0.036 739
23				H	0.049 186

<sup>a</sup> The schematic diagram above shows the structure of the AMP conformer. For PEAC, instead of a CH<sub>3</sub> group, a H atom appears at position 17.

used in conjunction with the atomic charges calculated at the present theory level.

Therefore, we proceed to modify the relevant  $A_{ij}^{\text{hb}}$  and  $C_{ij}^{\text{hb}}$  parameters for the 10–12 potential on the basis of the new ab initio calculated atomic charges presented in Table 1 and the new results for (H<sub>2</sub>O)<sub>2</sub>,<sup>11,18,19</sup> (NH<sub>3</sub>)<sub>2</sub>,<sup>11,20</sup> and NH<sub>3</sub>(H<sub>2</sub>O)<sub>1</sub>.<sup>11,21</sup> structures and energies. This allows a parameter fit for O–H...O, O–H...N, and O...H–N hydrogen-bonding structures to be achieved. Parameters thus fitted are based on the benchmark systems above and will serve to generate better modeling potentials for all hydrogen-bonded systems. Note that since the goal is to describe more complicated systems than these few phototypical benchmark dimers, the potentials must be based on isolated molecule geometries and charges. The value in eq 1 for  $D$  must be put to 1 for the best fit to the benchmark system. With the above algorithm, nearly 80% of the binding energy in a hydrogen-bonded system such as those above is due to the Coulomb terms in the potential energy function. The fitted  $A_{ij}^{\text{hb}}$  and  $C_{ij}^{\text{hb}}$  parameters are listed in Table 3. Using the newly fitted potentials, the binding energies of the benchmark systems are estimated within 10% of the ab initio results (Table 4), and the potential energy based geometry is also in reasonable agreement with the ab initio and experimental results (Figure 1).

The newly fitted parameters of Table 3 will not perfectly reproduce the ab initio or experimental results of these hydrogen-bonded model systems. As seen from Table 1, for example, the atomic charges for the water dimer are different from those of the water monomer, due to charge transfer between the two

**TABLE 3: Parameters Derived for Hydrogen-Bonding Interactions**

atom pair <sup>a</sup>	$A_{ij}^{\text{hb}}$ (kcal Å <sup>12</sup> /mol)	$B_{ij}^{\text{hb}}$ (Å <sup>10</sup> /mol)
H <sub>4</sub> ...O <sub>18</sub>	16 574	4 892
H <sub>2</sub> ...O <sub>18</sub>	50 443	11 120
H <sub>4</sub> ...N <sub>14</sub>	24 425	6 974
H <sub>2</sub> ...N <sub>14</sub>	487 374	76 433

<sup>a</sup> The subscripts denote the atom types as defined in Table 2 of ref 13d. H<sub>2</sub> is amine or amide hydrogen, H<sub>4</sub> is hydroxyl or carboxylic acid hydrogen, O<sub>18</sub> is hydroxyl or carboxylic (C–O–H) or ester (C–O–C) oxygen, and N<sub>14</sub> is amine or amide nitrogen.

**TABLE 4: Binding Energies of Various Clusters from Empirical and ab Initio Calculations (cm<sup>-1</sup>)**

cluster	ab initio	empirical
Ar...H <sub>2</sub> O	130.2 <sup>a</sup>	124
Ar...NH <sub>3</sub>	130.1 <sup>a</sup>	174
CO <sub>2</sub> ...CO <sub>2</sub>	484 <sup>b</sup>	459
C <sub>6</sub> H <sub>6</sub> ...H <sub>2</sub> O	854 <sup>c</sup>	907
H <sub>2</sub> O...H <sub>2</sub> O	1717 <sup>d</sup>	1942
H <sub>2</sub> O...NH <sub>3</sub> (HOH...NH <sub>3</sub> )	2109 <sup>e</sup>	2122
NH <sub>3</sub> ...NH <sub>3</sub>	1000 <sup>f</sup>	1234
PEAC...H <sub>2</sub> O	2574 <sup>g</sup>	2498
	1546 <sup>g</sup>	1568

<sup>a</sup> Reference 22. <sup>b</sup> Reference 23. <sup>c</sup> Reference 24. <sup>d</sup> References 18 and 19. <sup>e</sup> Reference 21. <sup>f</sup> Reference 20. <sup>g</sup> Reference 6.

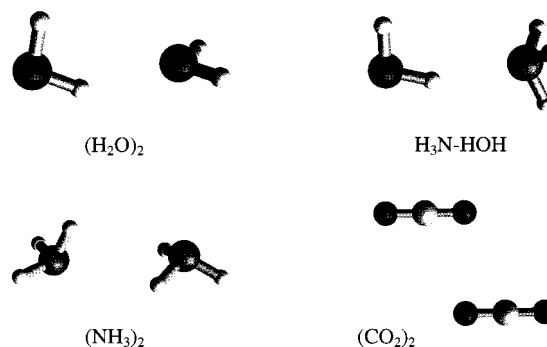


**Figure 1.** Geometries of some benchmark dimer systems calculated using the LJC model. The geometry and atomic charges of isolated monomers are calculated at the MP2/aug-cc-pVDZ or higher level, and are used in LJC modeling.

water molecules of the dimer. Thus, one could claim that hydrogen bonding is due to a charge transfer mostly between the two heavy atom centers between which the hydrogen atom is bonded. The geometry of the individual H<sub>2</sub>O molecules of the water dimer is also relaxed. Thus, while the model of the LJC potential energy surface is not exact for the benchmark systems, it is a faithful representation of these dimers and certainly a very convenient representation of more complex systems. The purpose of empirical potential models is not the reproduction of the properties of simple benchmark systems such as (H<sub>2</sub>O)<sub>2</sub>, (NH<sub>3</sub>)<sub>2</sub>, NH<sub>3</sub>(H<sub>2</sub>O)<sub>1</sub>, etc. Rather the idea is to generate a set of transferable parameters that can be used to model large, complicated systems that cannot presently be treated by ab initio theory at sufficiently high enough levels to generate reliable predictions.

### III. Results

#### A. Theoretical Results. 1. PEA and AMP Bare Molecules.

The geometries of PEA conformers are optimized at the MP2/6-311++G\*\* level with relaxation of all coordinates. The geometries calculated for the five (A–E) conformers are not significantly different from those presented in previous work.<sup>2,5,6</sup>

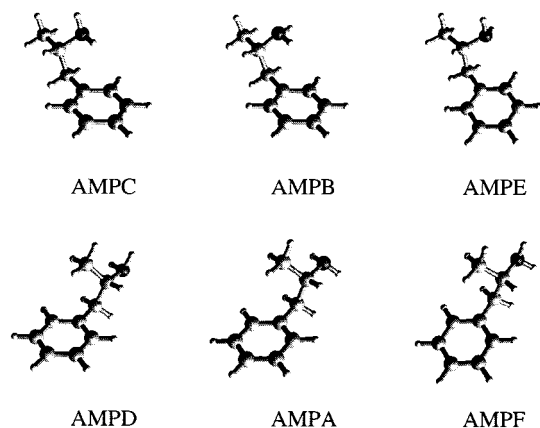


Figure 2. Geometries of AMP conformers calculated at the MP2/6-31++G\*\* level.

TABLE 5: Relative Energies (kJ/mol) of PEA and AMP Conformers at the MP2/6-311++G\*\* and MP2/6-31++G\*\* Levels, Respectively

conformer	PEA			AMP
	this work	ref 3 <sup>a</sup>	ref 6 <sup>b</sup>	this work
C (III)	0.00	0.00	0.00	0.00
B (II)	1.38	0.47	0.16	3.75
A (V)	5.85(5.75, <sup>c</sup> 6.25 <sup>d</sup> )	3.93	4.65	6.72
D (IV)	5.61(6.06 <sup>d</sup> )	5.58	5.85	7.16
E (I)	8.75	7.68	6.88	11.59
F				7.51

<sup>a</sup> At the MP2/6-31G\*\* level. <sup>b</sup> At the MP2/6-311G\*\* level. <sup>c</sup> At the MP2/6-31++G\*\* level. <sup>d</sup> At the /MP2/aug-cc-pVDZ level. <sup>e</sup> The Roman numerals refer to calculated conformers of refs 3, 5, and 6.

Similar calculations are performed for AMP at the MP2/6-31++G\*\* level. The primary structural difference between PEA and AMP is the substitution of a hydrogen atom by a methyl group on the  $\beta$  side chain carbon atom. If CH<sub>3</sub> is regarded as a free rotor, six basic conformer structures can be considered for AMP. Note that since the  $\beta$  carbon of AMP is chiral, AMP should have twelve conformers; energetically, however, only six of them can be distinguished. These six basic structures are shown in Figure 2. If the CH<sub>3</sub> group in the B, C, A, and E conformers of AMP is substituted by an H atom, the structures become B, C, A, and E conformers, respectively, of PEA. Similar substitution of CH<sub>3</sub> by an H atom in the D and F conformers of AMP generates the D conformer structure of PEA. Ab initio relative energies of the different conformers are presented in Table 5 for both PEA and AMP. For both molecules conformer C is suggested to be the most stable, and conformer E is suggested to be the least stable.

A note of caution should be sounded here. In all such calculations of conformer structures, the most compact structures are typically of the lowest energy. This is true here, and this trend is consistent with the notion that these compact gauche structures will have the largest BSSE problems. The NH<sub>2</sub> in this structure, for example, can best borrow basis set functions from the ring group (and, of course, vice versa) to lower the total energy of the structure. This BSSE correction will be much larger than that for the trans conformers in which the NH<sub>2</sub> and ring groups are quite separated. Unfortunately, one has no present straightforward algorithm for correcting this problem in single molecules, but at this level of theory, the BSSE correction for (H<sub>2</sub>O)<sub>2</sub>, (NH<sub>3</sub>)<sub>2</sub>, etc. would be ca. 8 kJ/mol;<sup>11</sup> this spread is well within the energy range of all the conformers.

2. PEA and AMP Clusters. The structures and binding energies for PEA and AMP conformer clusters with various

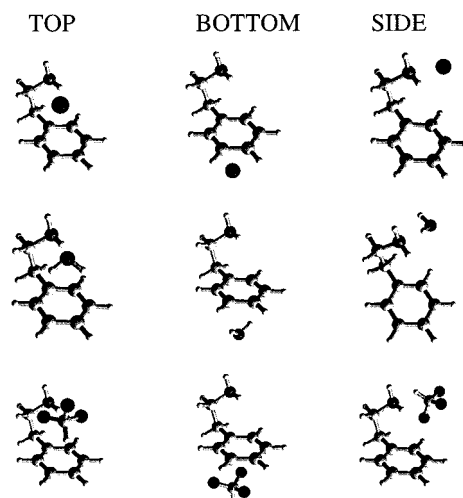


Figure 3. Structures of PEA clustered with Ar, H<sub>2</sub>O, and CF<sub>3</sub>H (upper, middle, and lower panels). Of the various isomers of the ring TOP, BOTTOM, and SIDE binding structures, only the one with the highest binding energy for each main binding site is shown.

solvents are calculated with the LJC potential function following the procedure outlined in section II.B. Some of the typical cluster isomer structures are shown in Figure 3, and the binding energies for some of the cluster isomers are listed in Table 6. As stated in section II, the atomic charges used for both solute conformers and solvent molecules are obtained from ab initio calculations. The geometries of the solvents are from experimental results, while those of the solute conformers are from ab initio results. The newly fitted  $A_{ij}^{hb}$  and  $C_{ij}^{hb}$  parameters for the 10–12 potential function are used for the calculation of hydrogen-bonding interactions. For each cluster system, LJC calculations reveal several local minimum binding structures. As shown in Figure 3, most of these isomer structures can be roughly divided into three types: (1) the ring TOP structure in which the solvent binds mainly to the phenyl ring and to the side chain; the solvent species and the side chain are on the same side of the ring; (2) the ring BOTTOM structure in which the solvent binds to the ring side away from the side chain; (3) the ring SIDE structure in which the solvent binds mainly to the NH<sub>2</sub> group on the side chain, and stays away from the ring top or bottom positions. Some low binding energy structures are also found for solvation in the ring plane if the solvent atoms are very electronegative and have large partial atomic negative charges.

The simplest case for PEA/solvent clusters is for an Ar solvent. For each PEA conformer, only one local minimum structure is found for each of the TOP, BOTTOM, and SIDE structures. The three isomers for PEA(Ar)<sub>1</sub> are shown in the top panel of Figure 3. The ring TOP structure appears to be the most stable one (largest binding energy), followed by the BOTTOM and the SIDE structures. The TOP PEA(Ar)<sub>1</sub> cluster has a binding energy of 559 cm<sup>-1</sup>, higher than that of the other conformer clusters, as can be seen in Table 6.

PEA clustered with CH<sub>4</sub>, CF<sub>4</sub>, and CF<sub>3</sub>Cl shows binding behavior similar to that of PEA(Ar)<sub>1</sub> (Table 6), with the most stable isomers assuming a ring TOP structure. The reduced symmetry of CF<sub>3</sub>Cl causes several additional local minimum structures for each type of general binding structure; these differ only by the change of CF<sub>3</sub>Cl orientation with respect to the PEA conformer. Typically, the barrier to interconversion among these isomer structures is small, and only the most stable ones will be considered. Only the largest binding energy for each binding type is listed in Table 6 for PEA(CH<sub>3</sub>Cl)<sub>1</sub>. The same

**TABLE 6: Binding Energies of PEA and AMP Clusters Estimated Using the LJC Potential<sup>a</sup>**

solvent	conformer	PEA <sup>b</sup>			AMP		
		TOP	BOTTOM	SIDE	TOP	BOTTOM	SIDE
Ar	C	552 (568)	469 (468)	345 (342)	570	474	400
	B	522	470	438	539	474	439
	A	564	467	371	506	474	404
N <sub>2</sub>	C	1015 (1043)	615 (613)	879 (875)	1038	617	909
	B	982	612	1041	1006	614	1043
	A	714	620	858	674	620	890
CH <sub>4</sub>	C	712 (725)	594 (592)	428 (425)	734	601	483
	B	673	595	636	692	602	493
	A	690	587	472	648	602	484
CF <sub>4</sub>	C	1098 (1111)	969 (964)	817 (796)	1122	982	909
	B	1084	970	616	1110	980	687
	A	1080	976	682	1060	983	695
CF <sub>3</sub> Cl	C	1209 (1225)	1136 (1130)	975 (946)	1237	1146	1058
	B	1238	1117	722	1270	1130	840
	A	1228	1135	796	1205	1104	849
CF <sub>2</sub> H <sub>2</sub>	C	955 (962)	874 (867)	964 (930)	970	842	1040
	B	926	856	845	969	858	862
	A	902	862	773	922	872	866
CF <sub>3</sub> H	C	975 (986)	931 (926)	913 (875)	993	935	1003
	B	998	923	810	1038	927	873
	A	946	957	771	989	940	893
CO <sub>2</sub>	C	1168 (1179)	1061 (1068)	996 (957)	1188	1071	1106
	B	1154	1063	938	1196	1065	932
	A	1188	1078	763	1164	1075	853
H <sub>2</sub> O	C	1619 (1568)	929 (943)	2623 (2498)	1598	934	2767
	B	1314	921	2534	1131	909	2650
	A	1049	996	2399	909	942	2591
CH <sub>3</sub> OH	C	2004 (1930)	1298 (1307)	3173 (2945)	1981	1313	3288
	B	1833	1282	2929	1826	1281	3112
	A	1396	1330	2802	1315	1287	3060
NH <sub>3</sub>	C	1597 (1569)	1011 (1015)	1507 (1469)	1599	1017	1579
	B	1427	998	1649	1498	993	1661
	A	1057	1037	1405	993	1011	1473

<sup>a</sup> The geometries and atomic charges used for PEA and AMP are calculated at MP2/6-31++G\*\* level. <sup>b</sup> Data in parentheses are estimated using PEAC geometry and atomic charges from MP2/aug-cc-pVDZ calculation. See Figure 3 for a pictorial reference of the meaning of "TOP", "BOTTOM", and "SIDE". See the text for a description of these structures.

practice will be followed for all the cluster systems with multiple local minima at a general binding type site.

Like PEA(CF<sub>3</sub>Cl)<sub>1</sub>, PEA clustered with CF<sub>3</sub>H and CF<sub>2</sub>H<sub>2</sub> shows multiple local minima for each of the TOP, BOTTOM, and SIDE binding types; however, additional binding can arise for PEAC(CF<sub>3</sub>H)<sub>1</sub> and PEAC(CF<sub>2</sub>H<sub>2</sub>)<sub>1</sub> between F atoms of the solvent and H atoms of the phenyl ring (Figure 3), arising from the high fluorine negative charges for CF<sub>3</sub>H and CF<sub>2</sub>H<sub>2</sub> (ca. -0.2). This additional interaction results in significantly higher binding energies for PEAC(CF<sub>3</sub>H)<sub>1</sub> and PEAC(CF<sub>2</sub>H<sub>2</sub>)<sub>1</sub> clusters compared to those for PEAA at this SIDE position, as seen from Table 6. The PEAC binding energies for these solvents can become as high as, or even higher than, those for the TOP binding positions of the other (PEAA) conformers.

The most stable cluster isomers for CO<sub>2</sub> clustered with all PEA conformers are found to have a ring TOP binding structure. A weak binding is also predicted between the O atom of CO<sub>2</sub> and a ring H atom in the SIDE binding structure for PEAC-(CO<sub>2</sub>)<sub>1</sub>. This cluster isomer structure has a binding energy of 996 cm<sup>-1</sup>, more than 200 cm<sup>-1</sup> higher than that of its PEAA counterpart.

Clusters of PEAA/N<sub>2</sub> appear to have higher binding energy in the SIDE binding structure than in the other two isomer structures, probably due to stronger binding between the NH<sub>2</sub> group and N<sub>2</sub>. The binding energies for the most stable isomers in SIDE, TOP, and BOTTOM structures are 857, 713, and 621 cm<sup>-1</sup>, respectively. The most stable isomer for PEAC(N<sub>2</sub>)<sub>1</sub> has a TOP binding structure, due to additional binding of N<sub>2</sub> to the NH<sub>2</sub> group. The corresponding binding energy is 1010 cm<sup>-1</sup>,

nearly 300 cm<sup>-1</sup> higher than that of the most stable TOP binding isomer of PEAA(N<sub>2</sub>)<sub>1</sub>.

The interaction between PEA and H<sub>2</sub>O is quite different from that discussed above for non-hydrogen-bonding solvents. Hydrogen bonding plays a major role in this case. For H<sub>2</sub>O clustered with all PEA conformers, a hydrogen bond can be formed between the NH<sub>2</sub> group of PEA and the H<sub>2</sub>O, much like for the case of the NH<sub>3</sub>(H<sub>2</sub>O)<sub>1</sub> dimer. H<sub>2</sub>O in such strong hydrogen-bonding structures assumes a position away from the ring (SIDE structure). The largest binding energies for PEA/H<sub>2</sub>O clusters are on the order of 2500 cm<sup>-1</sup>. For the ring TOP structures of PEAC(H<sub>2</sub>O)<sub>1</sub>, besides binding to the ring, the oxygen atom of water molecule also has some additional binding with a hydrogen atom of the NH<sub>2</sub> group, as shown in Figure 3. The PEAC(H<sub>2</sub>O)<sub>1</sub> TOP binding energy is 1631 cm<sup>-1</sup>. The binding energies for the BOTTOM structure of all PEA conformers with H<sub>2</sub>O are ca. 1000 cm<sup>-1</sup>. These general PEA/(H<sub>2</sub>O)<sub>1</sub> binding energies and structures are similar to those found by ab initio techniques.<sup>6</sup>

PEA/CH<sub>3</sub>OH clusters are, in general, predicted to be more stable than PEA/H<sub>2</sub>O clusters and also to have a number of local minima in each of the three main binding sites. These energies are given in Table 6.

The binding of NH<sub>3</sub> to PEA is quite complicated. NH<sub>3</sub> has a fairly strong hydrogen bond formation with the NH<sub>2</sub> group in PEA. Several SIDE binding cluster isomers with binding energies ca. 1300–1500 cm<sup>-1</sup> are found for all PEA conformers. Additional binding between the solvent and the NH<sub>2</sub> group is evident for the ring TOP structure of PEAC(NH<sub>3</sub>)<sub>1</sub>. Several ring

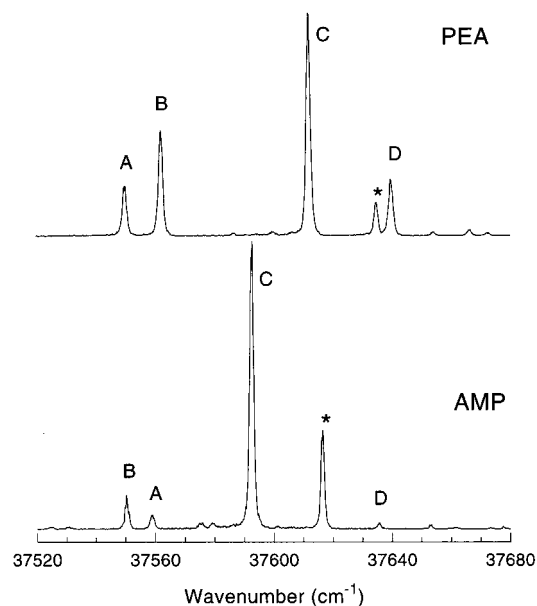


**Figure 4.** MRES spectra of the  $S_1 \leftarrow S_0$  transition of PEA and AMP. The asterisk denotes the cluster feature of  $\text{PEA}(\text{H}_2\text{O})_1$  or  $\text{AMPC}(\text{H}_2\text{O})_1$ . The same notation holds for all the following figures.

**TABLE 7:  $S_1 \leftarrow S_0$  Transition Origins of PEA and AMP ( $\text{cm}^{-1}$ )**

conformer	PEA	AMP	conformer	PEA	AMP
A	37 550	37 559	C	37 612	37 593
B	37 562	37 551	D	37 639	37 636

TOP isomers of  $\text{PEA}(\text{NH}_3)_1$  show binding energies comparable to those of the SIDE binding ones (see Table 6).

The binding patterns of AMP with various solvents are much the same as those for PEA. Most of the AMP cluster isomer structures have their counterparts in PEA clusters. The only structural difference between these two systems is the substitution of a  $\beta$  carbon site H atom in PEA by a  $\text{CH}_3$  group in AMP. To avoid redundancy, the structures of AMP clusters are not shown. The additional  $\text{CH}_3$  group on the side chain only slightly increases the cluster binding energies, as shown in Table 6. AMP clustered with  $\text{CF}_2\text{H}_2$  and  $\text{CF}_3\text{H}$  represent two exceptions by showing a slightly stronger SIDE binding configuration. Some local minimum structures can be found for AMP/solvent clusters with the solvent binding in the vicinity of the  $\beta$ - $\text{CH}_3$  group. The binding energies of such structures are much lower than the most stable ones found in the TOP, BOTTOM, and SIDE structures.

#### B. Experimental Results. 1. PEA and AMP Bare Molecules.

Figure 4 depicts the spectra of the  $S_1 \leftarrow S_0$  transition for the conformers of isolated PEA and AMP. All the transition origins fall in the range  $37540\text{--}37650\text{ cm}^{-1}$ , as is typical for a substituted benzyl chromophore (see Table 7). PEA has five possible conformers. The experimentally observed feature intensities are determined by both the intrinsic stability of the individual conformer and the experimental conditions (especially cooling). As shown in the upper panel of Figure 4, four features are observed for the PEA  $0_0^0$  transition in our supersonic jet experiment. These features are assigned as the A, B, C, and D conformers of PEA following the convention of previous work.<sup>3,5,6</sup> An additional feature, near peak D (ca.  $37\ 635\text{ cm}^{-1}$ ), arises from the fragmentation of  $\text{PEA}(\text{H}_2\text{O})_1$  into the PEA mass channel, as is confirmed by previous work,<sup>5,6</sup> as well as this work. The calculated least stable conformer E is not assigned in this work. These conformers are depicted in Figure 2 for the specific instance of AMP.

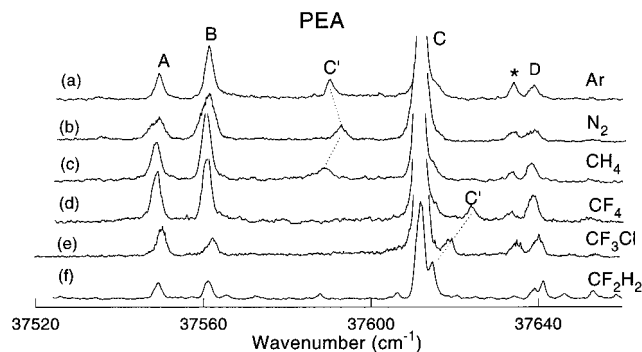


**Figure 5.** FE spectra of PEA clustered with (a) Ar, (b)  $\text{N}_2$ , (c)  $\text{CH}_4$ , (d)  $\text{CF}_4$ , (e)  $\text{CF}_3\text{Cl}$ , and (f)  $\text{CF}_2\text{H}_2$ . Cluster features are labeled with C'. Features labeled with A, B, C, and D arise from bare PEA.

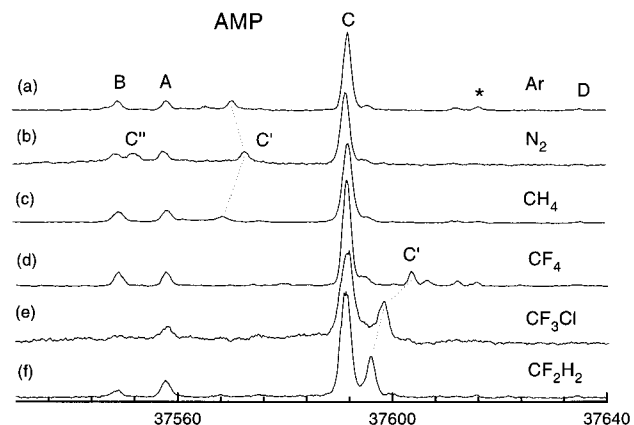


**Figure 6.** FE spectra of AMP clustered with (a) Ar, (b)  $\text{N}_2$ , (c)  $\text{CH}_4$ , (d)  $\text{CF}_4$ , (e)  $\text{CF}_3\text{Cl}$ , and (f)  $\text{CF}_2\text{H}_2$ . Features that arise from bare PEA conformers are labeled with A, B, C, and D. Features labeled with C' arise from 1:1 clusters of AMPC with these solvents. The feature labeled with C'' arises from  $\text{AMPC}(\text{N}_2)_2$ .

The lower panel in Figure 4 shows four features that can be attributed to four AMP conformers. The additional strong feature between peaks C and D (ca.  $37\ 617\text{ cm}^{-1}$ ) arises from the fragmentation of the  $\text{AMP}(\text{H}_2\text{O})_1$  cluster. We label the set of features for AMP in accordance with the PEA assignment of conformers, on the basis of the correlation between the two sets of features: their peak intensities, their cooling behavior, and their behavior under solvation conditions. We will discuss this further below. Most of the AMP spectral intensity is attributable to feature C, with very little intensity found for the conformer D feature. This is probably caused by the additional effect of the  $\beta$ -methyl group on the potential barriers separating different conformers.

Spectra of PEA and AMP are also observed in the mass channels of their respective fragments  $\text{CH}_2\text{NH}_2$  and  $\text{CHCH}_3\text{-NH}_2$ . Such fragmentation is quite severe for AMP, especially in one-color ionization detected spectra.

**2. PEA and AMP Clusters.** The solvation and fragmentation behaviors of PEA and AMP with various solvent molecules are very similar. This is perfectly understandable, given the structural similarity of the two molecules. In general, AMP and its clusters are more susceptible to fragmentation, due to the existence of the additional  $\text{CH}_3$  group on the  $\beta$  carbon in the side chain, which apparently aids in the stabilization of the fragment  $[\text{CHRCH}_2\text{NH}_2]^+$ .

Ar,  $\text{N}_2$ ,  $\text{CH}_4$ ,  $\text{CF}_4$ ,  $\text{CF}_3\text{Cl}$ , and  $\text{CF}_2\text{H}_2$ . Both FE and mass detected spectra are obtained for these clusters. Figures 5 and 6 show their FE spectra. These clusters all share the following properties and attributes: (1) their spectra all show only one

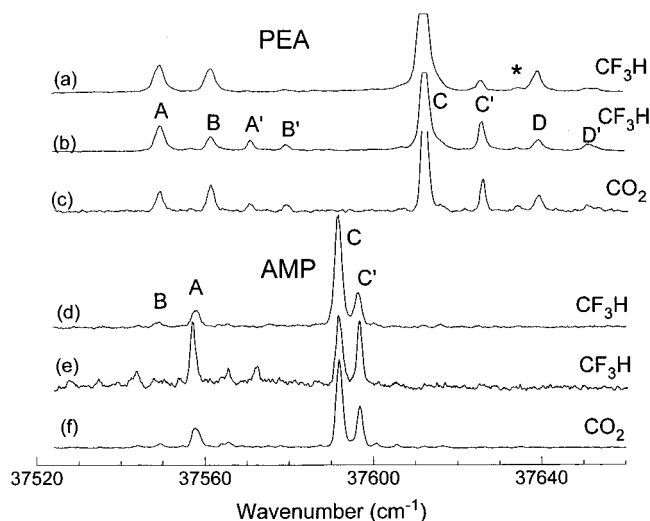


**Figure 7.** FE spectra of PEA and AMP clustered with  $\text{CF}_3\text{H}$  and  $\text{CO}_2$ . Features that arise from bare PEA and AMP conformers are labeled with A, B, C, and D. Corresponding cluster features are labeled with A', B', C', and D'. Spectra a and b are for  $\text{CF}_3\text{H}$  concentrations of 0.1% and 0.3%.

**TABLE 8:  $S_1 \leftarrow S_0$  Transition Origins of 1:1 vdW Clusters of PEA and AMP ( $\text{cm}^{-1}$ )**

solvent	conformer	PEA		AMP	
		origin	shift	origin	shift
Ar	C	37 590	-22	37 571	-22
$\text{N}_2$	C	37 592	-20	37 574	-19
$\text{CH}_4$	C	37 589	-23	37 569	-23
$\text{CF}_4$	C	37 624	12	37 605	12
$\text{CF}_3\text{Cl}$	C	37 619	7	37 600	7
$\text{CF}_2\text{H}_2$	C	37 615	3	37 598	5
$\text{CF}_3\text{H}$	A	37 571	21		
	B	37 580	18		
	C	37 626	14	37 598	5
	D	37 652	13		
$\text{CO}_2$	A	37 570	20		
	B	37 579	17		
	C	37 627	15	37 598	5
$\text{H}_2\text{O}$	A	37 595	45	37 575	25
	B	37 599	37	37 580	25
	C	37 635	23	37 617	24
	D	37 666	27	37 653	18
$\text{CH}_3\text{OH}$	B			37 568	18
	C	37 634	22	37 618	25
	D	37 666	27	37 653	18

feature, which most likely arises from a cluster of the C conformer of PEA (PEAC) and AMP (AMPC), respectively, and (2) the lone features are only detected in the PEA and AMP mass channels in MRES experiments, respectively. These clusters completely fragment into their bare chromophore, and its fragment mass channels, upon ionization.

Spectral shifts for PEA cluster features with regard to feature C of the PEA spectrum are -22, -20, -23, 12, 7, and 3  $\text{cm}^{-1}$ , respectively, while those for AMP cluster features with regard to feature C of the AMP spectrum are -22, -19, -23, 12, 7, and 5  $\text{cm}^{-1}$ , respectively (see Table 8).

As stated in Section III.A, LJC simulations of PEAC and AMP clusters with these solvents suggest three major binding structures for all conformers. For almost all these solvents, the most stable cluster structure is a ring TOP binding structure, with additional binding interactions to the side chain, especially the  $\text{NH}_2$  group. Most likely, this is the structure detected.

$\text{CF}_3\text{H}$ , and  $\text{CO}_2$ . As shown in Figure 7a–c, spectroscopic features can be observed for clusters of all four PEA conformers

with the two solvents  $\text{CF}_3\text{H}$  and  $\text{CO}_2$ , given appropriate experimental conditions. The spectral shifts are 22, 18, 15, and 13  $\text{cm}^{-1}$  for clusters of the A, B, C, and D conformers of PEA with  $\text{CF}_3\text{H}$ , and the spectral shifts are 12, 17, and 15  $\text{cm}^{-1}$  for clusters of the A, B, and C conformers of PEA with  $\text{CO}_2$  (Table 8). The cluster spectra of PEA with these two solvents are strikingly similar to one another.

The spectra of AMP/ $\text{CF}_3\text{H}$  and AMP/ $\text{CO}_2$  clusters are simpler, with only one feature identified for each case (Figure 7d–e). These lone features are most likely related to the AMPC conformer, and are both 5  $\text{cm}^{-1}$  red shifted with respect to the AMPC feature.

In MRES experiments, spectra of the PEA/solvent clusters are observed only in the PEA (and fragment) mass channels, indicating complete cluster fragmentation upon ionization. A difference between the PEA/ $\text{CF}_3\text{H}$  and PEA/ $\text{CO}_2$  and AMP/ $\text{CF}_3\text{H}$  and AMP/ $\text{CO}_2$  systems is that, in addition to strong features in the AMP mass channel, very weak features are also observed in the  $\text{CHCH}_3\text{NH}_2$  mass channel for AMPC clustered with  $\text{CO}_2$  and  $\text{CF}_3\text{H}$  solvents. Both a more stable fragment ion and better solvation of that ion by  $\text{CO}_2$  and  $\text{CF}_3\text{H}$  may be responsible for this latter observation.

As shown in Table 6, the binding energies of PEA and AMP clusters with  $\text{CF}_3\text{H}$  and  $\text{CO}_2$  are ca. 1000 and 1200  $\text{cm}^{-1}$ , respectively, as obtained by LJC potential energy calculations. The most stable cluster isomers formed by PEA conformers and AMPC with these two solvents have ring TOP binding structures, with the exception of  $\text{AMPC}(\text{CF}_3\text{H})_1$ , which shows virtually the same binding energy for the TOP and the SIDE binding (Figure 3 and Table 6). The most stable calculated cluster isomer for each of the PEA conformers is probably the one that is observed experimentally.

Note from Figures 4–7 that, with different cooling conditions, the relative intensity ratios of different PEA conformer peaks vary significantly. Under higher backing pressure, and with the seeding of higher concentrations of solvents, especially those that can serve as more effective coolants, the relative intensities of less stable conformers decrease dramatically. This is most obvious for a comparison of the intensities of features associated with conformers A and B. Feature B is much more intense than A for the bare molecule (Figure 4), but becomes much less intense than A for expansions with added  $\text{CF}_3\text{H}$  solvent (Figure 7). A more detailed analysis shows that the intensity ratios between the gauche conformers B and C and between the anti conformers D and A decrease upon these enhanced cooling conditions; however, the intensity ratio of A to C remains roughly the same. The relative intensities of cluster features appear to follow approximately the relative intensities of their parent conformers. Further analysis of this phenomenon will be presented in the Discussion section.

With the seeding of these solvents in the He backing gas, bare AMP conformer intensity ratios D/A and B/C also decrease (conformer features D and B become very weak).  $\text{CF}_3\text{H}$  and  $\text{CO}_2$  again appear to be better coolants and clustering agents. An extreme case for this conformer feature intensity change can be seen in Figure 7e: with 70 psi backing gas of 0.3%  $\text{CF}_3\text{H}$  in He, B and D conformer signals are completely quenched. C conformer intensity is also quenched significantly in this instance, perhaps because of enhanced overall clustering for this particular AMP/ $\text{CF}_3\text{H}$  solvent system.  $\text{AMP}(\text{CF}_3\text{H})_1$  and  $\text{AMP}(\text{CO}_2)_1$  evidence good intensity for only AMP conformer C, even under extreme cooling conditions. This observation suggests that conformer C of AMP is much more stable than the others. As shown above,  $\text{PEA}(\text{CF}_3\text{H})_1$  and  $\text{PEA}(\text{CO}_2)_1$



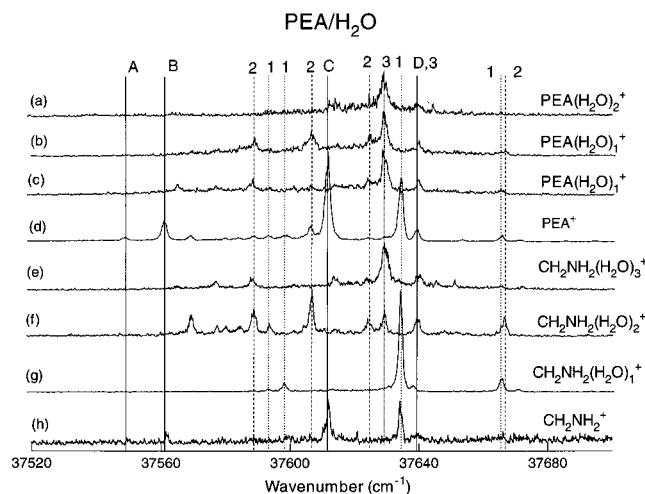


**Figure 8.** MRES of PEA clustered with H<sub>2</sub>O detected at various fragment mass channels. (a) and (b) are two-color spectra, while the rest are one-color spectra. Mass channels are (a) 157, (b, c) 139, (d) 121, (e) 84, (f) 66, (g) 48, and (h) 30 amu.

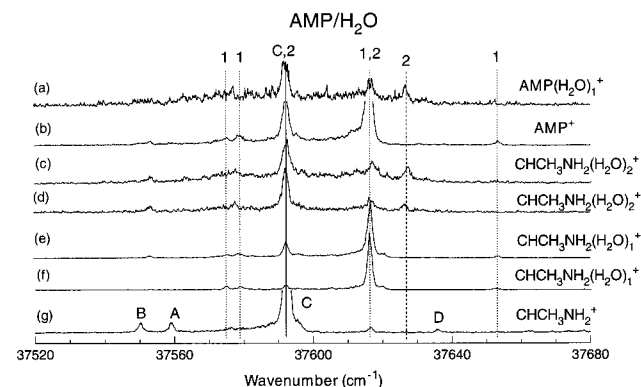


**Figure 9.** Two-color MRES of AMP clustered with H<sub>2</sub>O detected at various fragment mass channels. Mass channels are (a) 153, (b) 135, (c, d) 80, (e, f) 61, and (g) 44 amu.

clusters display features for all conformers. This difference in clustering behavior for PEA and AMP with CF<sub>3</sub>H and CO<sub>2</sub> can arise for two separate reasons: (1) conformer C of AMP is relatively more stable compared to its other conformers than is conformer C of PEA and (2) the barriers to conformer interconversion for PEA are higher than those for AMP. Of course, both conditions may be operative.

**H<sub>2</sub>O.** The solvation and ionic state fragmentation of PEA/H<sub>2</sub>O and AMP/H<sub>2</sub>O clusters are very complicated. MRES experiments reveal that, upon ionization, such clusters completely fragment into many different mass channels. Figures 8 and 9 present the spectra of PEA(H<sub>2</sub>O)<sub>n</sub> and AMP(H<sub>2</sub>O)<sub>n</sub> clusters detected in various mass channels. The spectra and their assignment of PEA(H<sub>2</sub>O)<sub>n</sub> are similar to those of ref 6. Nonetheless, to facilitate the systematic analysis of the general solvation patterns of PEA and AMP, we choose to present briefly the experimental results for PEA(H<sub>2</sub>O)<sub>n</sub>.

Four PEA(H<sub>2</sub>O)<sub>1</sub> features at 37 595, 37 599, 37 635, and 37 666 cm<sup>-1</sup> are identified, corresponding to one cluster with each of the four PEA conformers observed. Similarly, four AMP(H<sub>2</sub>O)<sub>1</sub> features can be identified at 37 575, 37 580, 37 617, and 37 653 cm<sup>-1</sup>, corresponding to 1:1 clusters with the B, A, C, and D conformers, respectively. For both PEA and AMP, although the features for the 1:1 clusters of conformer C with H<sub>2</sub>O are very intense, those of the other conformer clusters are weak.

The C<sub>6</sub>H<sub>5</sub>CH<sub>2</sub>CHRNH<sub>2</sub>(H<sub>2</sub>O)<sub>1</sub> clusters (where R=H and CH<sub>3</sub> for PEA and AMP, respectively) fragment into several mass channels, including C<sub>6</sub>H<sub>5</sub>CH<sub>2</sub>CHRNH<sub>2</sub><sup>+</sup>, [CHRNH<sub>2</sub>(H<sub>2</sub>O)<sub>1</sub>]<sup>+</sup>, and CHRNH<sub>2</sub><sup>+</sup>. This behavior is in contrast to the non-hydrogen-bonded clusters discussed above, which only fragment into the PEA mass channel. Again, the presence of a solvent molecule in the backing gas has a dramatic effect on the bare molecule conformer relative intensities. For CF<sub>3</sub>H and CO<sub>2</sub> solvent molecules, the conformer D/A and B/C bare molecule intensity ratios decrease with respect to those found for a pure He expansion. With H<sub>2</sub>O in the expansion gas, the A/C, B/C, and D/C intensity ratios for the bare conformers decrease dramatically with respect to those found for the pure He expansion. As can be seen in Figures 8d and Figure 9d, the PEAC and AMPC bare molecule intensity has become the predominant spectral feature for the He/H<sub>2</sub>O expansion (compare to Figure 4).

In Figure 8, four features, at 37 589, 37 607, 37 625, and 37 667 cm<sup>-1</sup>, arise from PEA(H<sub>2</sub>O)<sub>2</sub> clusters, while features at 37 630 and 37 640 cm<sup>-1</sup> likely arise from the PEA(H<sub>2</sub>O)<sub>3</sub> clusters. The 37 640 cm<sup>-1</sup> feature overlaps the D conformer origin of PEA. One cannot readily associate these features with specific PEA conformers. A careful comparison of spectra detected in different mass channels suggests that PEA(H<sub>2</sub>O)<sub>2</sub> fragments into [PEA(H<sub>2</sub>O)<sub>1</sub>]<sup>+</sup>, PEA<sup>+</sup>, and [CH<sub>2</sub>NH<sub>2</sub>(H<sub>2</sub>O)<sub>2</sub>]<sup>+</sup>, while PEA(H<sub>2</sub>O)<sub>3</sub> fragments into [PEA(H<sub>2</sub>O)<sub>2</sub>]<sup>+</sup>, [PEA(H<sub>2</sub>O)<sub>1</sub>]<sup>+</sup>, [CH<sub>2</sub>NH<sub>2</sub>(H<sub>2</sub>O)<sub>3</sub>]<sup>+</sup>, and [CH<sub>2</sub>NH<sub>2</sub>(H<sub>2</sub>O)<sub>2</sub>]<sup>+</sup> mass channels.

At least three features (at 37 593, 37 617, and 37 627 cm<sup>-1</sup>) appear to be related to AMP(H<sub>2</sub>O)<sub>2</sub> (Figure 9). They are detected in the [AMP(H<sub>2</sub>O)<sub>1</sub>]<sup>+</sup> and [CHCH<sub>3</sub>NH<sub>2</sub>(H<sub>2</sub>O)<sub>2</sub>]<sup>+</sup> mass channels; two of them accidentally overlap with AMPC and AMPC(H<sub>2</sub>O)<sub>1</sub> features.

As shown in Figure 3 and Table 6, LJC calculations suggest that the most stable cluster structure for PEA and AMP conformers with water has H<sub>2</sub>O hydrogen bonded to the NH<sub>2</sub> group away from the ring top position (SIDE structure). The ring TOP and BOTTOM structures are much less stable, with ca. 1000 cm<sup>-1</sup> less binding energy. Since only one 1:1 cluster feature is observed corresponding to each conformer, these features can best be assigned to the much stronger hydrogen-bonded SIDE binding cluster structures.

**CH<sub>3</sub>OH.** The mass-detected spectra of PEA(CH<sub>3</sub>OH)<sub>n</sub> and AMP(CH<sub>3</sub>OH)<sub>n</sub> clusters are presented in Figures 10 and 11. Fragmentation patterns shown in the figures are very similar to those shown in Figures 8 and 9 for PEA/H<sub>2</sub>O and AMP/H<sub>2</sub>O clusters.

Features at 37 634, and 37 666 cm<sup>-1</sup> in the PEA and CH<sub>2</sub>NH<sub>2</sub>(CH<sub>3</sub>OH)<sub>1</sub><sup>+</sup> mass channels (Figure 10d,g) can be assigned to PEA(CH<sub>3</sub>OH)<sub>1</sub> clusters corresponding to C and D conformers.

PEA(CH<sub>3</sub>OH)<sub>2</sub> clusters demonstrate two interesting phenomena. First, a series of three features at 37 604, 37 608, and 37 612 cm<sup>-1</sup>, with a separation between peaks of only 4 cm<sup>-1</sup>, is observed. The last feature accidentally overlaps with the PEAC transition origin. In one-color detection, these features appear not only in the 153 ([PEA(CH<sub>3</sub>OH)<sub>1</sub>]<sup>+</sup>, 121 (PEA<sup>+</sup>), and 94 ([CH<sub>2</sub>NH<sub>2</sub>(CH<sub>3</sub>OH)<sub>2</sub>]<sup>+</sup>) mass channels, but also in the 154 ([PEA(CH<sub>3</sub>OH)<sub>1</sub>H]<sup>+</sup>) mass channel. This progression may belong to a van der Waals torsional mode of a specific PEA(CH<sub>3</sub>OH)<sub>2</sub> isomer. Second, a feature at 37 666 cm<sup>-1</sup>, which has a higher signal intensity than the three-peak series in the 153 ([PEA(CH<sub>3</sub>OH)<sub>1</sub>]<sup>+</sup>) mass channel for two-color detection (Figure 10c), but has a much weaker intensity than for those three peaks in one-color detection (Figure 10b), does not appear in the 154 mass channel at all. One may suspect that the 37 666 cm<sup>-1</sup>

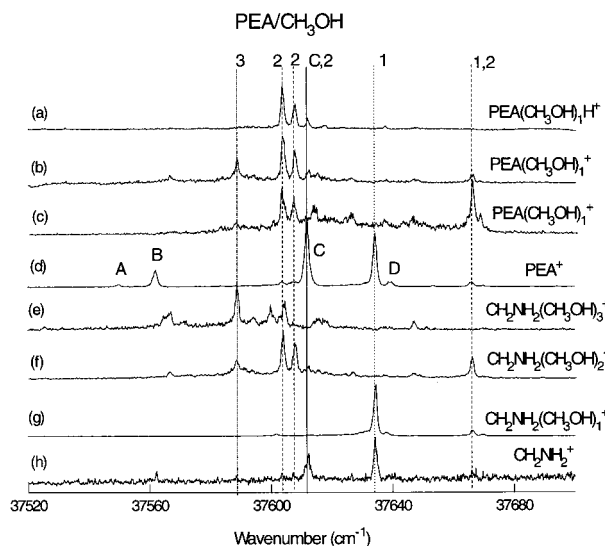


**Figure 10.** MRES of PEA clustered with  $\text{CH}_3\text{OH}$  detected at various fragment mass channels. (c) is a two-color spectrum, while the rest are one-color spectra. Mass channels are (a) 154, (b, c) 153, (d) 121, (e) 126, (f) 94, (g) 62, and (h) 30 amu.

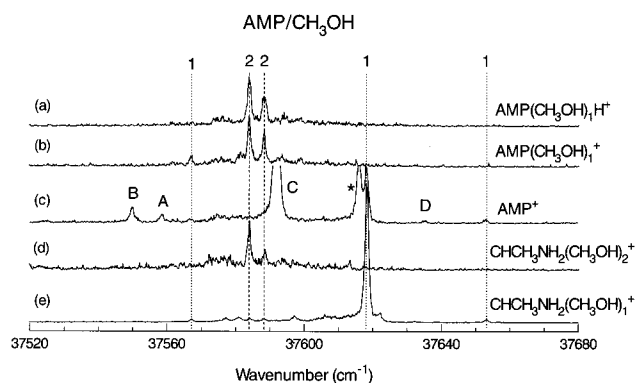


**Figure 11.** MRES of AMP clustered with  $\text{CH}_3\text{OH}$  detected at various fragment mass channels. (c) is a two-color spectrum, while the rest are one-color spectra. Mass channels are (a) 168, (b) 167, (c) 135, (d) 108, and (e) 76 amu.

feature arises from only  $\text{PEA}(\text{CH}_3\text{OH})_1$ ; however, as can be seen from one-color ionization detection in mass channel 94 ( $[\text{CH}_2\text{NH}_2(\text{CH}_3\text{OH})_2]^+$ , Figure 10f), this is definitely a feature associated with  $\text{PEA}(\text{CH}_3\text{OH})_2$ . Nonetheless, through comparison with the behavior of  $\text{PEA}(\text{H}_2\text{O})_{1,2}$  clusters at this energy ( $37\,666$  and  $37\,667\text{ cm}^{-1}$ ) and with the general result that PEA ion fragments tend not to lose hydrogen-bonding solvent, one can suggest that both  $\text{PEA}(\text{CH}_3\text{OH})_{1,2}$  clusters have features at  $37\,666\text{ cm}^{-1}$ . Therefore, the  $37\,666\text{ cm}^{-1}$  feature that appears in mass channel 153 arises mostly from  $\text{PEA}(\text{CH}_3\text{OH})_2$  fragmentation. The different fragmentation pattern of this feature compared to that of the three-peak series suggests that these features belong to two different types of  $\text{PEA}(\text{CH}_3\text{OH})_2$  clusters with different bonding interactions and, therefore, different structures.

Only one feature (at  $37\,589\text{ cm}^{-1}$ ) can be assigned to  $\text{PEA}(\text{CH}_3\text{OH})_3$  with confidence. The fragmentation of this cluster is also ionization energy dependent. One-color signals are observed in the  $[\text{PEA}(\text{CH}_3\text{OH})_1]^+$ ,  $[\text{CH}_2\text{NH}_2(\text{CH}_3\text{OH})_3]^+$ , and  $[\text{CH}_2\text{NH}_2(\text{CH}_3\text{OH})_2]^+$  mass channels. Apparently, loss of only one  $\text{CH}_3\text{OH}$  from this cluster is not an open channel at the energies employed.

The intense feature located at  $37\,618\text{ cm}^{-1}$  in Figure 11 appears in both the  $\text{AMP}^+$  and  $[\text{CHCH}_3\text{NH}_2(\text{CH}_3\text{OH})_1]^+$  mass

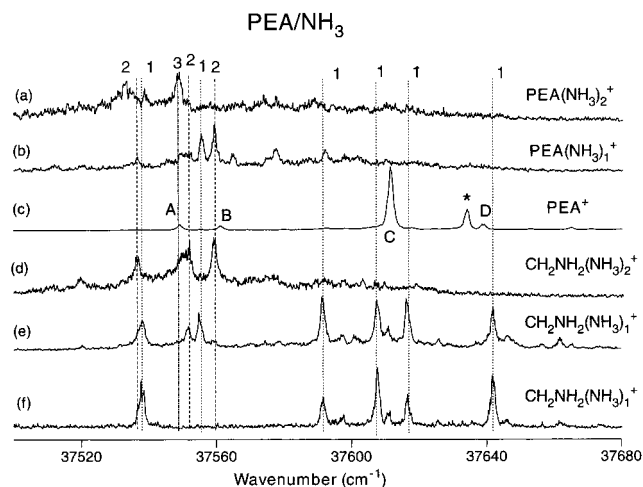


**Figure 12.** MRES of PEA clustered with  $\text{NH}_3$  detected at various fragment mass channels. (f) is a two-color spectrum, while the rest are one-color spectra. Mass channels are (a) 155, (b) 138, (c) 121, (d) 64, and (e, f) 47 amu.

channels and can be assigned as the  $\text{AMPC}(\text{CH}_3\text{OH})_1$  band origin. Two very weak features, at  $37\,565$  and  $37\,653\text{ cm}^{-1}$ , show behavior similar to that of the intense  $\text{AMPC}(\text{CH}_3\text{OH})_1$  feature. They are likely cluster peaks related to the B and D conformers of AMP. The spectral shifts of these three features with respect to the B, C, and D origins of AMP are 18, 25, and  $18\text{ cm}^{-1}$ .

$\text{AMP}(\text{CH}_3\text{OH})_2$  shows a series of features in the mass channels of several  $\text{AMPC}/\text{CH}_3\text{OH}$  fragments including  $[\text{AMP}(\text{CH}_3\text{OH})_1]^+$ ,  $[\text{AMP}(\text{CH}_3\text{OH})_1\text{H}]^+$ , and  $[\text{CHCH}_3\text{NH}_2(\text{CH}_3\text{OH})_2]^+$ . Two clearly identified features of this series are separated by  $4\text{ cm}^{-1}$ , and this suggests the existence of an isomer structure for this cluster similar to that posed for  $\text{PEA}(\text{CH}_3\text{OH})_2$ . Note, however, that the counterpart of the third  $\text{PEA}(\text{CH}_3\text{OH})_2$  feature is not observed for  $\text{AMP}(\text{CH}_3\text{OH})_2$ .

LJC simulations suggest an interaction pattern for the 1:1 clusters of PEA and AMP with  $\text{CH}_3\text{OH}$  very similar to that found for the corresponding clusters formed with  $\text{H}_2\text{O}$ . The most stable configuration (SIDE) has an  $\text{N}\cdots\text{H}-\text{O}$  hydrogen bond with the  $\text{CH}_3\text{OH}$  solvent away from the phenyl ring. The TOP configuration for this cluster is much less stable.

$\text{NH}_3$ . The spectra of  $\text{PEA}(\text{NH}_3)_n$  and  $\text{AMP}(\text{NH}_3)_n$  are very complicated and very different from those of the other clusters. Five features can be associated with the  $\text{PEA}(\text{NH}_3)_1$  (Figure 12). They all have large and comparable intensities in the  $[\text{CH}_2\text{NH}_2(\text{NH}_3)]^+$  mass channel. Four relatively prominent features appear to be associated with the  $\text{AMP}(\text{NH}_3)_1$  cluster (Figure 13), with one of them overlapping the  $\text{AMPC}$  band origin. As discussed above, cluster features observed for all but the C conformer of PEA show weak intensities. Cluster features show no specific pattern for their spectral shifts with regard to the PEA conformer features. Additionally, cluster features of all conformers show similar spectral shifts. Given these facts, these strong  $\text{PEA}(\text{NH}_3)_1$  features most likely do not arise from different PEA conformers.

LJC potential energy simulations reveal that several possible TOP and SIDE configurations exist for  $\text{NH}_3$ -related clusters with binding energies in the range  $1300\text{--}1500\text{ cm}^{-1}$ . This is in contrast to the results of LJC potential energy simulations for  $\text{H}_2\text{O}$ -related clusters for which the most stable SIDE configuration is more than  $1500\text{ cm}^{-1}$  lower in energy than the next most stable cluster configuration. Thus, several cluster structures may coexist in the expansion for the  $\text{PEA}(\text{NH}_3)_1$  and  $\text{AMP}$ -

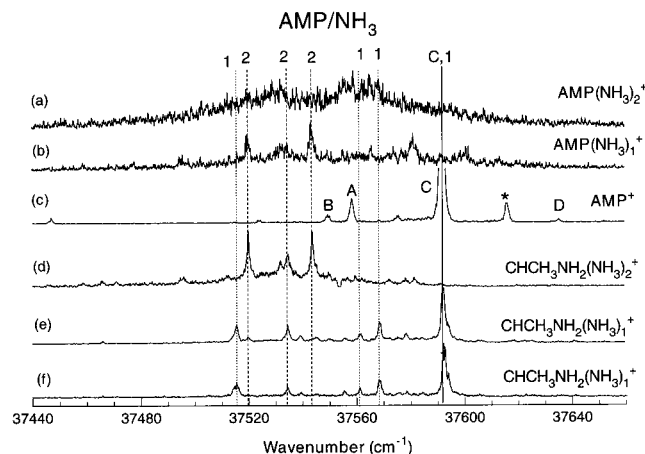


**Figure 13.** MRES of AMP clustered with  $\text{NH}_3$  detected at various fragment mass channels. (d) and (f) are two-color spectra, while the rest are one-color spectra. Mass channels are (a) 169, (b) 152, (c) 135, (d) 78, and (e, f) 61 amu.

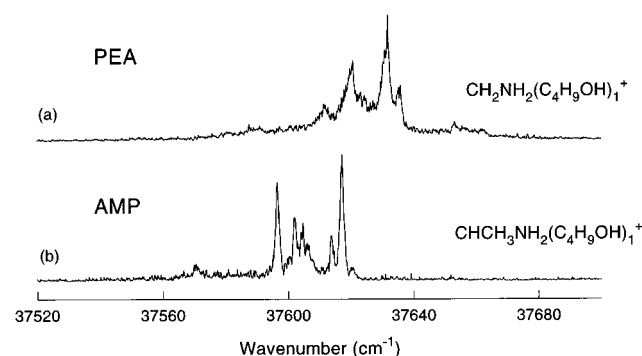


**Figure 14.** MRES spectra of PEA and AMP clustered with  $\text{C}_4\text{H}_9\text{OH}$  detected at their fragment mass channels: (a) 104 and (b) 118 amu.

$(\text{NH}_3)_1$  clusters and may contribute to the multifeatured spectrum observed for this system.

The fragmentation of the  $\text{NH}_3$ -related clusters is different from that of the  $\text{H}_2\text{O}$ - and  $\text{CH}_3\text{OH}$ -related clusters discussed above. Mass-resolved spectra are only detected in the  $[\text{CHRNH}_2(\text{NH}_3)_1]^+$  mass channel in both one-color and two-color experiments.

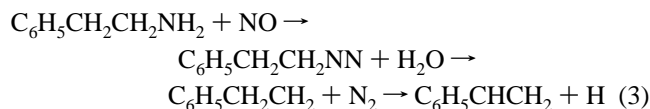
Three features are observed in the  $[\text{PEA}(\text{NH}_3)_1]^+$  and  $[\text{CH}_2\text{NH}_2(\text{NH}_3)_2]^+$  mass channels. These features probably arise from  $\text{PEA}(\text{NH}_3)_2$ , and are labeled “2” in Figure 12. Another sizable feature is observed only in the  $[\text{PEA}(\text{NH}_3)_2]^+$  channel. This feature may belong to larger  $\text{PEA}/\text{NH}_3$  and is labeled “3” in Figure 12.

Three additional peaks are found to be associated with  $\text{AMP}(\text{NH}_3)_2$  (see Figure 13). They can be observed in the  $\text{AMP}(\text{NH}_3)_1^+$ ,  $[\text{CHCH}_3\text{NH}_2(\text{NH}_3)_2]^+$ , and  $[\text{CHCH}_3\text{NH}_2(\text{NH}_3)_1]^+$  mass channels in one-color MRES.

**Isobutanol.** The spectrum of PEA and AMP clustered with  $\text{C}_4\text{H}_9\text{OH}$  is only observed in  $[\text{CHRNH}_2(\text{C}_4\text{H}_9\text{OH})_1]^+$  mass channels, as shown in Figure 14. Both spectra contain a group of broad features. Only the  $\text{C}_6\text{H}_5\text{CHRNH}_2(\text{C}_4\text{H}_9\text{OH})_1$  cluster appears to be formed in this experiment. Upon ionization, the clusters all fragment into the  $[\text{CHRNH}_2(\text{C}_4\text{H}_9\text{OH})_1]^+$  mass channel.

**3. Reactions with NO.** With only 0.1% NO gas seeded in the He backing gas, the spectra of bare PEA and AMP are completely quenched. Instead of PEA and AMP spectra, other features can be observed in MRES experiments. These spectra do not relate to cluster signals since they are not observed in

any of the relevant mass channels. These fairly strong signals can only be observed in mass channels 93 and 104 for PEA, and in mass channels 93 and 118 for AMP. A further investigation of spectra obtained from these mass channels confirms that these spectra arise from the excitation of  $\text{C}_6\text{H}_5\text{NH}_2$ ,  $\text{C}_6\text{H}_5\text{CHCH}_2$  (styrene), and  $\text{C}_6\text{H}_5\text{CHCHCH}_3$  from their ground states to their first excited single states. This suggests that instead of forming clusters with NO, PEA and AMP react with NO. Using PEA as an example, the following possible reaction path may be responsible for  $\text{C}_6\text{H}_5\text{CHCH}_2$  formation:



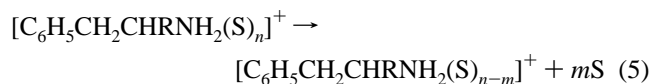
Because the spectrum of styrene shows that the styrene is cold, and because the PEA signal completely vanishes with NO in the beam, we expect that this reaction occurs in the nozzle for the PEA ground state. Aniline ion  $\text{C}_6\text{H}_5\text{NH}_2^+$  is detected in the same manner for both PEA and AMP. Again, the  $\text{C}_6\text{H}_5\text{NH}_2^+$  detected signal is indicative of cold aniline, and in the absence of NO in the expansion gas, little or no ( $\leq 1$  mV) aniline signal is observed in mass channel 93. Exactly how  $\text{C}_6\text{H}_5\text{NH}_2$  is formed from NO and PEA or AMP is not fully understood.

#### IV. Discussion

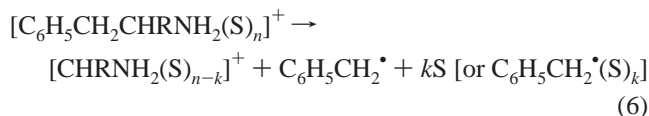
**A. Relative Energies of the Conformers.** PEAC is the most stable of all the PEA conformers; however, the relative energy levels of the two anti conformers PEAA and PEAD are not as clear. MP2 level calculations show that the two anti conformers A and D have very similar relative ground-state energies with respect to PEAC. With a 6-311G\*\* or smaller basis set, the relative energy of PEAA is ca. 1.0–2.0 kJ/mol lower than that of PEAD, while with basis sets of 6-311++G\*\* and aug-cc-pVDZ, the relative energy of PEAA is ca. 0.2 kJ/mol higher than that of PEAD. Given the fact that these basis sets may lead to a basis set superposition error as high as ca. 8 kJ/mol, one cannot draw a firm conclusion about the relative levels of PEAA and PEAD based on the ab initio calculation results.

The spectral intensities of the PEAA and PEAD  $S_1 \leftarrow S_0$  transition are almost the same for the bare molecule PEA (Figure 4). This indicates that the relative energy levels of the two conformers should be nearly the same. The fact that PEAA and its clusters show more intense features than their PEAD counterparts with  $\text{CF}_3\text{H}$  and  $\text{CO}_2$  as solvents indicates a higher ground-state population for the PEAA conformer. This suggests a higher stability for PEAA and its clusters compared to their PEAD counterparts.

**B. Fragmentation Patterns.** From section III we have seen that, in MRES experiments, all PEA and AMP clusters experience fragmentation upon ionization. The general ion fragmentation patterns of AMP and its clusters are very similar to those of PEA and its clusters. To simplify the discussion, we use S to represent solvent molecules. Then the basic fragmentation paths are represented as



and



In these equations,  $n = 1, 2, \text{ or } 3$ ,  $m = 1 \text{ or } 2$ , and  $k = 0 \text{ or } 1$ , depending on each individual case.

Both PEA and AMP bare molecules fragment following reaction 4. This path involves the breaking of the  $\alpha$ - $\beta$  carbon-carbon bond; AMP undergoes more severe fragmentation, apparently due to the additional stabilization effect for the  $CHRNH_2^+$  ion by the  $CH_3$  group.

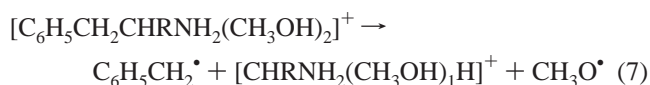
PEA and AMP clusters all show complete fragmentation into lower mass channels, with reactions 5 and 6 apparently the main paths. The specific pattern and relative path intensities for each cluster depend on the solvent involved.

Only path 5 is observed for PEA clustered with Ar,  $N_2$ ,  $CH_4$ ,  $CF_4$ ,  $CF_3Cl$ , and  $CF_2H_2$  with  $n = m = 1$  for most cases. In these systems the  $\alpha$ - $\beta$  carbon-carbon bond is not broken in the cluster ion dissociation.  $CF_3H$  and  $CO_2$  solvents apparently provide sufficient ion stabilization that a benzyl radical is formed and ring to solvated side chain ( $CHRNH_2(S)_n$ ) charge transfer occurs, generating path 6 at low intensity. The only fragment ion for this channel with  $S = CF_3H$  and  $CO_2$  is  $CHCH_3NH_2^+$  rather than  $CHCH_3NH_2^+(S)_1$ .

If  $S$  is a hydrogen-bonding solvent, such as  $H_2O$  and  $CH_3OH$ , both paths 5 and 6 are active: the same cluster feature for a particular isomer cluster appears in the fragment mass channel corresponding to both dissociation reactions. The relative intensity distribution of the feature in these fragment mass channels depends largely on the ionization laser energy. With high ionization laser energy (one-color ionization) path 6 is favored, especially for AMP clusters. A hydrogen-bonding solvent and the added  $\beta$ - $CH_3$  group provide additional stability to the  $CHRNH_2$  fragment, as the  $[CHCH_3NH_2(S)_{n-k}]^+$  ion is formed.

A few special cases can be noted, in addition, that probably arise because the rates of reactions 5 and 6 become comparable for a particular set of conditions. For example, if  $S = NH_3$ , the fragmentation of  $[C_6H_5CH_2CHRNH_2(NH_3)_n]^+$  follows path 6 for  $n = 1$ . If  $n > 1$ , the cluster fragmentation reaction occurs along both paths 5 and 6.

Another interesting special fragmentation occurs for  $[C_6H_5CH_2CHRNH_2(CH_3OH)_2]^+$ . In this instance both paths 5 and 6 are active, but the additional fragmentation reaction occurs as follows:



To try to rationalize and understand these molecular and cluster fragmentation patterns, consider a schematic energy level diagram for the clusters as given in Figure 15. The left half of the diagram depicts the potential energy curves of  $C_6H_5CH_2CHRNH_2(S)_1$  along the van der Waals bond coordinate ( $C_6H_5CH_2CHRNH_2-S$ ), while the right half of the figure depicts the potential curves of the cluster along the bond between the  $\alpha$  and  $\beta$  carbon atoms of the side chain ( $C_6H_5CH_2-CHRNH_2(S)_1$ ). If the solvent  $S$  is neglected, the right side of the diagram also applies to PEA and AMP bare molecules. Note that since cluster ions are much more tightly bound than  $S_1$  state van der Waals clusters in their equilibrium configurations, curve I (for the cluster ion) indicates a stronger binding with a deeper potential well compared to that of its  $S_1$  state counterpart.

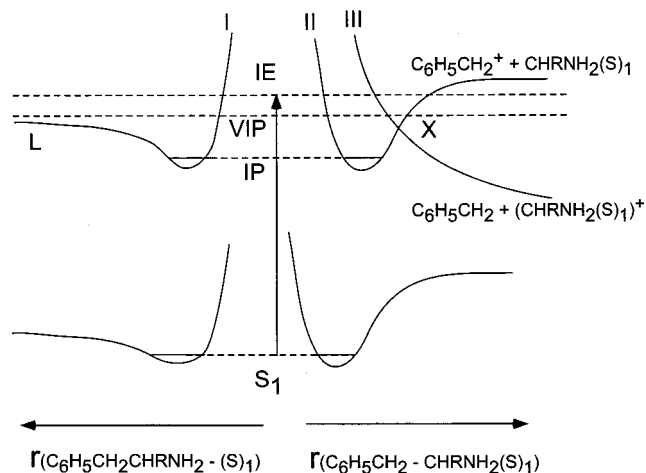


**Figure 15.** Schematic potential curves of  $C_6H_5CH_2CHRNH_2(S)_1$  at  $S_1$  and ionic states. Left half: potential energy versus the length of the van der Waals bond. Right half: potential energy versus the  $\alpha$ - $\beta$  carbon-carbon bond length.

Both PEA and AMP, as well as their clusters, have a very gradual rise in their photo ion yield versus wavelength curves: signal intensity increases very gradually over the ionization laser wavelength range of 310–290 nm. This suggests a significant geometry relaxation of these species upon ionization.<sup>7</sup> This geometry relaxation (through the Franck-Condon factor for the  $I \leftarrow S_1$  transition) results in a significantly larger vertical ionization energy (VIP) than the adiabatic ionization energy, as indicated in the diagram. To ionize a molecule, the ionization laser energy (IE) must be high enough to reach the VIP level ( $IE \geq VIP$ ). Ions generated are obviously vibrationally excited with excess energy distributed in various modes. Even with a “threshold” ionization ( $IE = VIP$ ), a cluster has enough excess energy ( $VIP - IP$ ) to fragment completely into the various fragment channels.

Consider first threshold ionization of clusters. From the left part of the diagram, we can see that if the VIP level is sufficiently higher than the dissociation threshold  $L$  of the van der Waals potential well (I), enough excess energy may be redistributed into the van der Waals stretching mode to lead to cluster ion fragmentation through path 5, that is, loss of one or more solvent molecules.

Fragmentation through path 6 actually involves a charge-transfer process. We know that the photoexcitation occurs at the benzyl ring chromophore. Upon ionization, the positive charge should be initially located at the ring. The corresponding potential curve can be represented by curve II on the right side of Figure 15. Curve III represents the repulsive potential leading to the products from path 6. These two curves (II and III) cross or mix at X. If VIP is sufficiently higher than the X level, upon threshold ionization, the cluster ion can cross from potential curve II to curve III, transfer an electron to the ring position from the amine group position, and dissociate along curve III. For nonthreshold ionization, IE, rather than VIP, should be used to analyze the fragment patterns.

For PEA and AMP, the excess energy absorbed during ionization is apparently redistributed in the  $\alpha$ - $\beta$  carbon-carbon bond stretching mode and perhaps other related modes. This leads to the crossing from curve II to curve III, resulting in fragmentation following path 4. The reaction is driven as well by the stability of the products:  $C_6H_5CH_2^\bullet$  and  $CHRNH_2^+$ . Whether the fragmentation of a cluster follows the main paths (5 or 6) or both or even others depends on the relative positions of the various potential energy surfaces, as well as the detailed

kinetics. For clusters of the neurotransmitters with non-hydrogen-bonding solvents, such as Ar, N<sub>2</sub>, and CF<sub>4</sub>, the van der Waals interaction is weak. The complete fragmentation, even at threshold ionization, suggests that the VIP level is higher than the L level. On the other hand, clusters of such solvents have a ring TOP configuration, which suggests a very limited stabilization effect to the [CHRNH<sub>2</sub>(S)<sub>n</sub>]<sup>+</sup> ion. Thus, potential surface III, and consequently the position X for such a case, is high in energy; in this instance, the VIP energy may be significantly lower than the X energy. Only enough excess energy is transferred into the van der Waals stretching mode to cause cluster fragmentation according to path 5. At the same time, path 6 is effectively shut down. Most of the clusters with non-hydrogen-bonding solvents fall in this category.

As for AMPC(CF<sub>3</sub>H)<sub>1</sub> and AMPC(CO<sub>2</sub>)<sub>1</sub>, the ring TOP configuration and the SIDE configuration show comparable binding energies. Due to the gauche structure of the C conformer, the solvent molecules can bind to the NH<sub>2</sub> group either from outside the ring (SIDE) or from the ring TOP position. Either way, along with the CH<sub>3</sub> group, this solvation can stabilize and induce charge transfer to generate the CHCH<sub>3</sub>-NH<sub>2</sub><sup>+</sup> moiety. The X level may thus be lowered. The balance of energy redistribution may therefore shift slightly, and lead to some minor fragmentation through path 6, as observed. Through RRKM theory, these energy considerations also lead to changes in relative rate constants for the various dissociation reactions.

On the other hand, the strong solvation effect of H<sub>2</sub>O and CH<sub>3</sub>OH on PEA and AMP at the end group of the side chain can effectively lower the X energy. Both L and X energies can now be lower than the VIP energy level; thereby, both paths 5 and 6 are opened. With the increase of ionization laser energy, path 6, i.e., the dissociation via crossing to potential surface III, becomes more favored. This switching between paths 5 and 6, depending on the laser ionization energy, is observed as larger signals for cluster spectra in the [CHRNH<sub>2</sub>(S)<sub>n-k</sub>]<sup>+</sup> mass channels for one-color MRES (large IE) than for two-color MRES (small IE).

Apparently [C<sub>6</sub>H<sub>5</sub>CH<sub>2</sub>CHRNH<sub>2</sub>(C<sub>4</sub>H<sub>9</sub>OH)<sub>1</sub>]<sup>+</sup> represents the other extreme. Strong solvation (hydrogen bonding) makes the X energy low and the L energy high. Within the ionization laser wavelength range we scanned, the corresponding IE is probably always higher than the X energy, and lower than the L energy. Thus, we can observe fragmentation following path 6, but not path 5. This may also be the case for [C<sub>6</sub>H<sub>5</sub>CH<sub>2</sub>CHRNH<sub>2</sub>(NH<sub>3</sub>)<sub>1</sub>]<sup>+</sup>, which fragments the same way as [C<sub>6</sub>H<sub>5</sub>CH<sub>2</sub>CHRNH<sub>2</sub>(C<sub>4</sub>H<sub>9</sub>OH)<sub>1</sub>]<sup>+</sup>.

LJC modeling results appear to support structurally the above analysis. Calculations show that H<sub>2</sub>O and CH<sub>3</sub>OH form strong hydrogen bonds with PEA and AMP at the NH<sub>2</sub> site. Breaking the α-β carbon-carbon bond is thus feasible on the basis of the cluster structure. There is no need to transfer the solvent from the ring top site to the lone pair site of -NH<sub>2</sub> upon fragmentation along path 6, and such solvents can have a strong stabilization effect for the positive charge on the RNH<sub>2</sub><sup>+</sup> moiety. The geometry and stabilization can facilitate charge transfer from the ring site to the NH<sub>2</sub> site, and facilitate the formation of the [CHRNH<sub>2</sub>(S)<sub>n</sub>]<sup>+</sup> ion. Moreover, C<sub>6</sub>H<sub>5</sub>CH<sub>2</sub>• itself is a very stable radical. Thus, potential surface III is not very high in energy, the crossing point X will have a lower energy than VIP, and fragmentation path 6 becomes accessible.

On the other hand, weakly bound clusters, such as PEA and AMP with Ar, N<sub>2</sub>, CH<sub>4</sub>, and CF<sub>4</sub>, tend to have ring TOP structures and have only a small interaction between the solvent

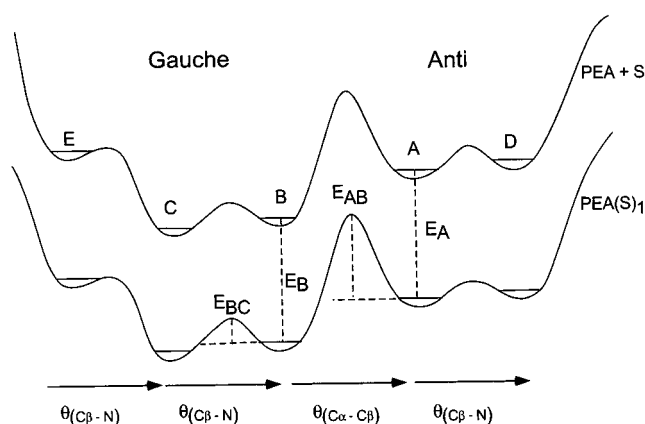


**Figure 16.** Schematic potential curves of PEA(S)<sub>1</sub>. Upper panel: the PEA molecule is separated from S by an infinite distance. Lower panel: the PEA molecule and the S molecule are at the equilibrium distance in a cluster. The angles  $\theta_{C\beta-N}$  and  $\theta_{C\alpha-C\beta}$  depict the coordinates along which the conversion of one conformer to another occurs. The conversion among anti or gauche conformers is realized through the change in the  $\theta_{C\beta-N}$  coordinate, that is, the rotation of the NH<sub>2</sub> group around the bond between the  $\beta$  carbon and the nitrogen. The conversion of an anti conformer to a gauche conformer, or vice versa, is through the change in the  $\theta_{C\alpha-C\beta}$  coordinate, that is, the rotation of the CHRNH<sub>2</sub> group around the bond between the  $\alpha$  and  $\beta$  carbon atoms.

and the terminal NH<sub>2</sub> group. Thus, in such clusters one would not expect any stabilization for α-β carbon-carbon bond scission or charge transfer from the ring to the -NH<sub>2</sub> moiety following cluster ionization.

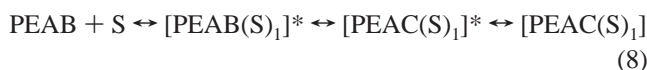
### C. Cooling and Solvation Effects on Spectral Intensity.

We have shown in section III that relative signal intensities of different conformers of PEA and AMP, as well as their clusters, vary according to the backing gas pressure and the solvent used. The general trend is that enhanced cooling and solvation conditions result in the decrease of the intensity ratio of peaks B/C and D/A for bare solute molecule features, as can be seen from Figures 4–6, 11, and 12. This is best seen in the case of PEA clusters for solvents CF<sub>3</sub>H and CO<sub>2</sub> (Figure 6); however, the relative intensity ratio of A to C does not show an obvious decrease under these cooling (solvation) conditions. On the other hand, expansion of PEA and AMP with hydrogen-bonding solvents, such as H<sub>2</sub>O, CH<sub>3</sub>OH, and others, not only causes the intensity ratios B/C and D/A to decrease, but also causes the intensity ratio A/C to decrease.

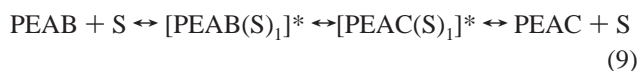
A schematic diagram, such as that given in Figure 16, may help to elucidate the relative intensities of different features under the various conditions described above. The lower curve depicts the minimum energy path on the potential surface for ground-state PEA conformers clustering with a solvent molecule (S). The path passes through the equilibrium position of all the conformer clusters. The upper curve depicts the minimum energy path for the conformer potential energy surface of the bare molecules with an infinite separation between the solute and solvent. Letters A–D represent the four observed conformers of PEA. E<sub>A</sub> and E<sub>B</sub> represent the binding energies of PEAA and PEAB clusters, while E<sub>AB</sub> and E<sub>BC</sub> represent the barriers for PEAA transforming to PEAB, and PEAB to PEAC, etc. [According to the MP2/6-31G\*\* calculations by Godfrey et al.,<sup>3</sup> E<sub>BC</sub>, E<sub>AD</sub>, and E<sub>AB</sub> are ca. 1140, 1120, and 1530 cm<sup>-1</sup>, respectively.] The two anti conformers are at the right side of the figure, and the two gauche conformers are at the left side of the figure. Conformer A is the most stable of the anti conformers, and C is the most stable of all conformers. One

conformer can transform to another one through the rotation of relevant functional groups along certain bonds, as indicated in the figure.

The intensities of the spectral features of solute conformers and their clusters depend on their ground-state populations. In the molecular beam, the cooling and clustering process starts at the nozzle exit, and continues until the beam density drops to the point at which no more collisions occur. Take PEAB and PEAC as examples. Population of solute conformers and their clusters in the beam are determined by three factors: (1) the distribution among conformers governed by beam density and temperature,  $\text{PEAB} \leftrightarrow \text{PEAC}$ , (2) the energy balance between a conformer and its cluster,  $\text{PEAB} + \text{S} \leftrightarrow [\text{PEAB}(\text{S})_1]^* \leftrightarrow \text{PEAB}(\text{S})_1$ , and (3) the conversion from one conformer and its cluster to another conformer and its cluster during the collision, cooling, and clustering process. During cluster formation, the excess energy (binding plus kinetic) must be removed through additional collisions to form a stable ground-state cluster. The overall cluster/conformer behavior can be illustrated as follows:



or



In principle, the excess energy in  $[\text{PEAB}(\text{S})_1]^*$  can be more than the binding energy  $E_B$ , and the excess energy may be transferred to the torsion mode of the bond between the solute  $\beta$  carbon and N. If the energy transferred into the torsion mode is large enough to overcome the barrier ( $E_{BC}$ ) on the minimum energy path between PEAB and PEAC, a conversion from  $[\text{PEAB}(\text{S})_1]^*$  to  $[\text{PEAC}(\text{S})_1]^*$  is possible. Further collisions will result in  $[\text{PEAC}(\text{S})_1]^*$  to be either stabilized to  $[\text{PEAC}(\text{S})_1]$  or fragmented to PEAC and S. Similar conversion and redistribution processes may also happen between other relevant conformer pairs. Obviously, conformers and clusters lower in energy should gain more population in such a process. In the case of  $\text{PEA}(\text{CF}_3\text{H})_1$ , the binding energy is estimated at ca.  $1000 \text{ cm}^{-1}$ , which may provide enough energy to overcome lower barriers such as  $E_{AD}$  and  $E_{BC}$ , but not enough to overcome higher barriers such as  $E_{AB}$ . Therefore, conversion and population redistribution may be restricted within the left and right wells of Figure 16, but little, if any, conversion or redistribution might occur between gauche and anti conformers. On the other hand, the binding energy of  $\text{PEA}(\text{H}_2\text{O})_1$  is as high as ca.  $2500 \text{ cm}^{-1}$ . Probably enough energy can be transferred to the relevant torsion mode to overcome both barriers  $E_{BC}$  and  $E_{AB}$ . Conversion and population redistribution may thus become possible among all the conformers and their clusters. Therefore, we observe an intensity ratio decrease for all other conformers with respect to conformer C for this clustering pair. The same analysis applies to AMP conformers and their clusters.

**D. Biological Relevance?** To the best of our knowledge, the conformational and cluster phenomena discussed above are especially pronounced in AMP and PEA, especially the conformational interconversions and specific conformer/cluster formation. Can any of this different behavior attributed to these “neurotransmitter” molecules be biologically relevant? A number of issues can be raised in this regard: Are conformations locked in at 1–10 K for isolated species relevant to room-temperature solutions? Is solvation behavior for clusters relevant

to solution solvation? Do the considerable entropy effects found in water solutions and proteins override the enthalpy/energy effects found for isolated systems? Are the assumed “lock and key” relationships between neurotransmitters and transmembrane proteins dependent on molecular conformations or on specific site binding interactions? At this point in our studies of neurotransmitter conformations and solvation, one cannot address these issues definitively. We trust that future studies of neurotransmitters such as dopamine, serotonin, adrenaline, noradrenaline, histamine, ... in a similar vein will allow us to comment on at least some of the points raised above.

## V. Conclusions

Spectral studies of the solvation and related chemistry of PEA and AMP are pursued by using FE and MRES techniques. Ab initio and atom–atom LJC potential energy surface calculations are performed to assist with the analysis of the experimental results. Some general conclusions can be stated as follows.

(1) The observed dependence of relative spectral intensities of PEA and AMP conformers and their clusters on the cooling conditions (backing pressure and coolants used) suggests that thermal and dynamic population redistribution can occur among these species in the cooling and clustering process. The amount of excess energy (binding energy) available through the clustering process plays a major role in the conformational conversions of PEA and AMP during cluster formation. With solvents that can have strong interactions (hydrogen bonding) with PEA and AMP, the redistribution of population among the conformers is among all conformers and their clusters. For weakly interacting solvents, the conformer redistribution is restricted within the anti or gauche conformer sets and their clusters.

(2) All PEA and AMP clusters studied experience fragmentation upon ionization. The small slopes of observed photo ion yield intensity curves versus ionization laser energy suggest a significant relaxation of the geometry of both PEA and AMP, as well as their clusters, following ionization. Consequently, the high vertical IP leads to high excess energy in the vibrational modes of the ions formed, causing fragmentation of clusters through a number of paths: loss of solvent molecules, breaking of the side chain  $\alpha$ – $\beta$  carbon–carbon bond, and  $\alpha$ – $\beta$  carbon–carbon bond breaking with additional loss of solvent molecules. Those clusters with weaker solute/solvent binding tend to fragment through the first path, while those forming hydrogen bonds tend to favor the latter two. The second path is strongly favored in AMP/solvent clusters due to the additional stabilization effect of the  $\text{CH}_3$  group at the  $\beta$  carbon position.

(3) Ab initio calculation results of several benchmark dimers are used to fit hydrogen-bonding parameters employed in the atom–atom LJC potential. The fitting of hydrogen-bonding structures and energies suggests that such strong bonding mainly arises from the strong Coulomb interactions among atoms with large partial atomic charges. With new ab initio atomic charges, newly fitted hydrogen-bonding parameters, cluster geometries, and binding energies are simulated using LJC potential energy functions. These simulated structures and binding energies are very helpful in interpreting the experimental results.

(4) Reactions are observed for PEA and AMP with NO present in the expansion gases. NO can completely quench PEA and AMP bare molecule signal intensity. The reaction products include  $\text{C}_6\text{H}_5\text{CH}=\text{CH}_2$  and  $\text{C}_6\text{H}_5\text{NH}_2$  for PEA, and  $\text{C}_6\text{H}_5\text{CH}=\text{CHCH}_3$  and  $\text{C}_6\text{H}_5\text{NH}_2$  for AMP.

**Acknowledgment.** This work is supported in part by the National Science Foundation and Army Research Office. We

thank Professor Anthony K. Rappé for many helpful discussions on intermolecular interactions and their calculation by ab initio, empirical, and semiempirical potential energy surface techniques.

## References and Notes

- (1) Sipior, J.; The, C. K.; Sulkes, M. *J. Fluoresc.* **1991**, *1*, 41.
- (2) Martinez, S. J., III; Alfano, J. C.; Levy, D. H. *J. Mol. Spectrosc.* **1993**, *158*, 82.
- (3) Godfrey, P. D.; Hatherley, L. D.; Brown, R. D. *J. Am. Chem. Soc.* **1995**, *117*, 8204.
- (4) Sun, S.; Bernstein, E. R. *J. Am. Chem. Soc.* **1996**, *118*, 5086.
- (5) Dickinson, J. A.; Hockridge, M. R.; Kroemer, R. T.; Robertson, E. G.; Simons, J. P.; McCombie, J.; Walker, M. *J. Am. Chem. Soc.* **1998**, *120*, 2622.
- (6) Hockridge, M. R.; Robertson, E. G. *J. Phys. Chem. A* **1999**, *103*, 3618.
- (7) (a) Li, S.; Bernstein, E. R. *J. Chem. Phys.* **1992**, *97*, 804. (b) Wanna, J.; Menapace, J. A.; Bernstein, E. R. *J. Chem. Phys.* **1968**, *85*, 1795. (c) Shang, Q. Y.; Moreno, P. O.; Li, S.; Bernstein, E. R. *J. Chem. Phys.* **1993**, *98*, 1876. (d) Shang, Q. Y.; Moreno, P. O.; Dion, C.; Bernstein, E. R. *J. Chem. Phys.* **1993**, *98*, 6769.
- (8) (a) Hobza, P.; Zahradnik, R. *Chem. Rev.* **1988**, *88*, 871. (b) Buckingham, A. D.; Fowler, P. W.; Hutson, J. M. *Chem. Rev.* **1988**, *88*, 963. (c) Hobza, P.; Selzle, H. L.; Schlag, E. W. *Chem. Rev.* **1994**, *94*, 1767. (d) Stone, A. J. *The Theory of Intermolecular Forces*; Oxford University Press: Oxford, 1996.
- (9) (a) Dykstra, C. E.; Andrews, L. *J. Chem. Phys.* **1990**, *92*, 6043. (b) Olthof, E. H. T.; van der Avoird, A.; Wormer, P. E. *S. J. Chem. Phys.* **1994**, *101*, 8430.
- (10) (a) Fernández, J. A.; Yao, J.; Bernstein, E. R. *J. Chem. Phys.* **1997**, *107*, 3363. (b) Yao, J.; Fernández, J. A.; Bernstein, E. R. *J. Chem. Phys.* **1997**, *107*, 8813. (c) Fernández, J. A.; Yao, J.; Bernstein, E. R. *J. Chem. Phys.* **1999**, *110*, 5159. (d) Yao, J.; Fernández, J. A.; Bernstein, E. R. *J. Chem. Phys.* **1999**, *110*, 5174. (e) Menapace, J. A.; Bernstein, E. R. *J. Phys. Chem.* **1987**, *91*, 2533.
- (11) Bernstein, E. R.; Rappé, A. K. *J. Phys. Chem.*, submitted for publication.
- (12) (a) Disselkamp, R.; Bernstein, E. R. *J. Chem. Phys.* **1993**, *98*, 4339. (b) Disselkamp, R.; Bernstein, E. R. *J. Phys. Chem.* **1994**, *98*, 7260. (c) Sun, S.; Bernstein, E. R. *J. Phys. Chem.* **1996**, *100*, 11348.
- (13) (a) Scott, R. A.; and Scheraga, H. A. *J. Chem. Phys.* **1966**, *45*, 2091. (b) Momany, F. A.; Carruthers, L. M.; McGuire, R. F.; Scheraga, H. A. *J. Phys. Chem.* **1974**, *78*, 1595. (c) Momany, F. A.; McGuire, R. F.; Burgess, A. W.; Scheraga, H. A. *J. Phys. Chem.* **1975**, *79*, 2361. (d) Némethy, G.; Pottle, M. S.; Scheraga, H. A. *J. Phys. Chem.* **1983**, *87*, 1883. (e) Scott, R. A.; Scheraga, H. A. *J. Chem. Phys.* **1965**, *42*, 2209.
- (14) *Handbook of Chemistry and Physics*, 79th (1998–1999) ed.; CRC Press: Boca Raton, FL, 1999.
- (15) Rappé, A. K.; Casewit, C. J.; Colwell, K. S.; Goddard, W. A., III; Skiff, W. M. *J. Am. Chem. Soc.* **1992**, *114*, 10026.
- (16) *Gaussian 98*, Revision A.6: Frisch, M. J.; Trucks, G. W.; Schlegel, H. B.; Scuseria, G. E.; Robb, M. A.; Cheeseman, J. R.; Zakrzewski, V. G.; Montgomery, Jr., J. A.; Stratmann, R. E.; Burant, J. C.; Dapprich, S.; Millam, J. M.; Daniels, A. D.; Kudin, K. N.; Strain, M. C.; Farkas, O.; Tomasi, J.; Barone, V.; Cossi, M.; Cammi, R.; Mennucci, B.; Pomelli, C.; Adamo, C.; Clifford, S.; Ochterski, J.; Petersson, G. A.; Ayala, P. Y.; Cui, Q.; Morokuma, K.; Malick, D. K.; Rabuck, A. D.; Raghavachari, K.; Foresman, J. B.; Cioslowski, J.; Ortiz, J. V.; Stefanov, B. B.; Liu, G.; Liashenko, A.; Piskorz, P.; Komaromi, I.; Gomperts, R. Martin, R. L.; Fox, D. J.; Keith, T.; Al-Laham, M. A.; Peng, C. Y.; Nanayakkara, A.; Gonzalez, C.; Challacombe, M.; Gill, P. M. W.; Johnson, B.; Chen, W.; Wong, M. W.; Andres, J. L.; Gonzalez, C.; Head-Gordon, M.; Replogle, E. S.; Pople, J. A., Gaussian, Inc., Pittsburgh, PA, 1998.
- (17) Wiberg, K. B.; Rablen, P. R. *J. Comput. Chem.* **1993**, *14*, 1504.
- (18) (a) Fellers, R. S.; Leforestier, C.; Braly, L. B.; Brown, M. G.; Saykally, R. J. *Science* **1999**, *284*, 945. (b) Curtiss, L. A.; Blander, M. *Chem. Rev.* **1988**, *88*, 827.
- (19) (a) Feyerisen, M. W.; Feller, D.; Dixon, D. A. *J. Phys. Chem.* **1996**, *100*, 2993. (b) Hess, O.; Caffarel, M.; Huiszoon, C.; Claverie, P. *J. Chem. Phys.* **1990**, *92*, 6049. (c) Smith, B. J.; Swanton, D. J.; Pople, J. A.; Schaefer, H. F., III; Random, L. *J. Chem. Phys.* **1990**, *92*, 1240. (d) Nielsen, I. M. B.; Seidl, E. T.; Janssen, C. L. *J. Chem. Phys.* **1999**, *110*, 9435.
- (20) (a) Tao, F.; Klemperer, W. *J. Chem. Phys.* **1993**, *99*, 5976. (b) Muguet, F. F.; Robinson, G. W. *J. Chem. Phys.* **1995**, *102*, 3648.
- (21) (a) Donaldson, D. J. *J. Phys. Chem. A* **1999**, *103*, 62. (b) Rablen, P. R.; Lockman, J. W.; Jorgensen, W. L. *J. Phys. Chem. A* **1998**, *102*, 3782. (c) Marten, B.; Kim, K.; Cortis, C.; Friesner, R. A.; Murphy, R. B.; Ringnalda, M. N.; Sitkoff, D.; Honig, B. *J. Phys. Chem.* **1996**, *100*, 11775.
- (22) Tao, F.; Klemperer, W. *J. Chem. Phys.* **1994**, *101*, 1145.
- (23) Bukowski, R.; Sadlej, J.; Jezioski, B.; Jankowski, P.; Szalewicz, K.; Kucharski, S. A.; Williams, H. L.; Rice, B. M. *J. Chem. Phys.* **1999**, *110*, 3785.
- (24) Courty, A.; Mons, A.; Dimicoli, I.; Piuze, F.; Gaigeot, A.; Brenner, V.; de Pujo, P. *J. Phys. Chem. A* **1988**, *102*, 6590.